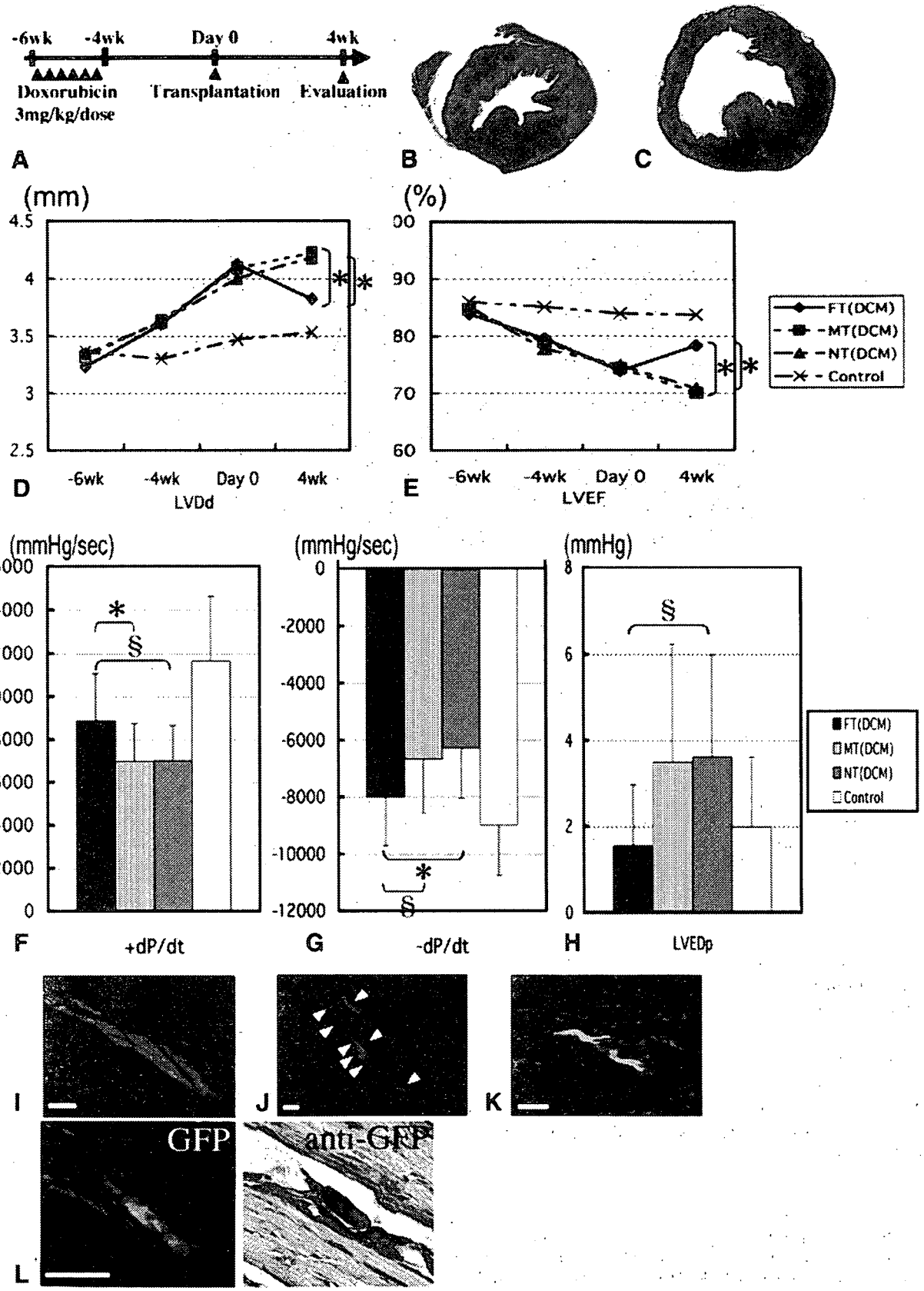
-6wk
-4wk
Day 0
4wk
Doxorubicin
3mg/kg/dose
Transplantation
Evaluation
A
B
C
(mm)
4.5
4
3.5
3
2.5
-6wk
-4wk
Day 0
4wk
LVDd
D
(%)
100
90
80
70
60
-6wk
-4wk
Day 0
4wk
LVEF
E
FT(DCM)
MT(DCM)
NT(DCM)
Control
(mmHg/sec)
16000
14000
12000
10000
8000
6000
4000
2000
0
+dP/dt
F
(mmHg/sec)
0
-2000
-4000
-6000
-8000
-10000
-12000
-dP/dt
G
(mmHg)
8
6
4
2
0
LVEDp
H
FT(DCM)
MT(DCM)
NT(DCM)
Control
I
J
K
GFP
anti-GFP
L

the large population of freshly sorted Flk1$^+$ cells expressed Sca-1 and c-kit (Fig. 1B), which are cardiac stem/progenitor cell markers [20]. In addition, the expression of Nanog and Oct4, which are undifferentiated ES cell markers, was significantly lower than in day 4 sorted Flk1$^-$ cells (Fig. 1C). By day 10 after differentiation, 12,000 Flk1$^+$ and Flk1$^-$ cells yielded 640±353 and 46±15 contractile colonies, respectively ($p<0.01$) (Fig. 1D). We used RT-PCR to assess whether these Flk1$^+$ cell derivatives expressed various cardiac markers. The day 4 sorted Flk1$^+$ cells expressed GATA-4 and Nkx2.5, which are cardiac markers that are detected from an early stage in the developing heart, and did not express the mature ventricular cell marker MLC2v, the atrial cell marker MLC2a, or the gap junction marker Cx43 (Fig. 2A). In contrast, day 4 sorted Flk1$^-$ cells did not express any of these markers (Fig. 2A). The day 10 Flk1$^+$ cell derivatives express MLC2a, MLC2v and Cx43 at significantly greater levels than the day 10 Flk1$^-$ cell derivatives. Immunohistochemical analysis also demonstrated that the day 10 contractile colonies expressed MLC2v, the developing cardiac cell and atrial cell marker ANP, sarcomeric protein MF20 and the cardiac troponin-I (cTn-I) (Fig. 2B–F). We next measured the electrical potentials of contractile colonies derived from Flk1$^+$ cells. The contractile colonies had action potentials as assessed by the MED64 system (Fig. 2G). By day 10 of differentiation, 500 Flk1$^+$ and Flk1$^-$ cells yielded 90.3±43.0 and 8.0±2.5 DiI-Ac-LDL-staining sheet-like endothelial colonies ($p<0.01$) (Fig. 1E). Similarly, 12,000 Flk1$^+$ and Flk1$^-$ cells yielded 228.0±59.2 and 16.3±6.3 hematopoietic clusters, identified by their cobblestone appearance by day 10 of differentiation ($p<0.01$) (Fig. 1F). That Flk1$^+$ cells differentiated more frequently into hematopoietic cells than Flk1$^-$ cells was also confirmed by FACS analysis of the CD45 expression on day 10 of differentiation (13.0% versus 0.8%) (Fig. 1G). Thus, when compared to Flk1$^-$ cells, Flk1$^+$ cells have a significantly greater potential to differentiate into not only hematopoietic and endothelial cells but also into mature cardiomyocytes, indicating that Flk1$^+$ cells are much closer to cardiac stem/progenitor cells than Flk1$^-$ cells.

3.2. Flk1+ cell transplantation improves cardiac function in DCM model mice

To investigate whether Flk1$^+$ cells undergo cardiomyogenesis in vivo as efficiently as they do in vitro, and whether cardiac function improves after Flk1$^+$ cell transplantation, we sorted Gact4-derived Flk1$^+$ cells on day 4 of differentiation and injected them directly into the hearts of DCM model mice. A total of 67 mice were used in these experiments: 20 DCM mice were transplanted with Flk1$^+$ cells [the FT(DCM) group], 19 DCM mice were injected with medium alone [the MT(DCM) group], 14 DCM mice were untreated [the NT (DCM) group], and 14 normal mice were used as controls (normal control). To assess the severity of the dilated cardiomyopathy in the DCM mice, LVDd and LVEF were assessed by echocardiography at −6 wks, −4 wks, day 0 and 4 wks. At −6 wks, −4 wks and day 0, all three DCM groups showed equivalent LVDd values which were significantly larger than the values for the normal control group (Fig. 3B, C). At 4 wks post-transplantation, the FT (DCM) group had significantly smaller LVDd values than the MT(DCM) and NT(DCM) groups (3.82±0.18 versus 4.22±0.22 and 4.0±0.19 mm, respectively) (Fig. 3D). The three DCM groups showed equivalent declining LVEF values until 4 wks post-transplantation, at which point the FT (DCM) group recovered significantly higher LVEF values than observed in the MT(DCM) and NT(DCM) groups (78.4±7.3 versus 70.1±5.0 and 70.9±5.6%, respectively) (Fig. 3E). However, the change in LVDd and LVEF values in the FT(DCM) group at 4 wks did not reach statistical significance when compared to their day 0 LVDd and LVEF values.

Cardiac catheterization was used to evaluate the + dP/dt and − dP/dt parameters and left ventricular end-diastolic pressure (LVEDp) at 4 wks post-transplantation. The FT (DCM) group showed significant improvements in their + dP/dt, − dP/dt and LVEDp values when compared to the values of the MT(DCM) and NT(DCM) groups (Fig. 3F–H). Thus, FT (DCM) group had significantly faster + dP/dt values than the MT(DCM) group and NT(DCM) groups (8858.3±2197.3 versus 6967.5±1765.7 and 6986.7±1645.3 mm Hg/s, respectively) (Fig. 3F), slower − dP/dt values (−8008.3±1706.9 versus −6673.9±1899.0 and −6289.1±1771.6 mm Hg/s, respectively) (Fig. 3G), and lower LVEDp values (1.54±1.42 versus 3.50±2.74 and 3.61±2.37 mm Hg, respectively) (Fig. 3H). These results indicate that Flk1$^+$ cell transplantation improved the systolic and diastolic cardiac function of DCM mice. Notably, when nine DCM mice were transplanted with Flk1$^-$ cells, their cardiac function did not improve at 4 wks post-transplantation as judged by echocardiography and cardiac catheterization (LVDd: 4.30±0.32 mm; LVEF: 71.5±4.8%; + dP/dt: 6771.5±1416.1 mm Hg/s; − dP/dt: −6585.4±1478.6 mm Hg/s; LVEDp: 6.2±4.8 mm Hg).

Furthermore, we evaluated the cardiac function of each group at 10 wks after cell transplantation. A slight improvement in the cardiac function of the FT(DCM) group ($n=3$) was still observed compared to that of the MT(DCM) ($n=3$) or NT(DCM) ($n=3$) groups at this time point [LVDd: 3.83±

Fig. 3. Transplantation of Flk1$^+$ cells into DCM mice significantly improves cardiac function. (A) Timeline of DCM mouse model generation and transplantation experiments. (B–C) Cross-sections of the left ventricle at the level of the papillary muscle of a normal 14 wk-old mouse (B) and a DCM mouse just prior to Flk1$^+$ cell transplantation (C). (D–H) The FT(DCM) group generally showed significant improvements in their LVDd (D), LVEF (E), + dP/dt (F), − dP/dt (G), and LVEDp values (H) compared to the MT(DCM) and NT(DCM) groups. *: $p<0.01$; §: $p<0.05$. (I) Fluorescence detection of groups of engrafted GFP$^+$ cells 4 wks after cell transplantation. (J) The image of lower magnification around the engrafted GFP$^+$ cells. The arrowheads in (J) indicates engrafted GFP$^+$ cells along the scar area resulting from cell injection. (K) Engrafted GFP$^+$ cells were also clearly detected in FT(DCM) mouse hearts 10 wks after cell transplantation. (L) GFP$^+$ cells (left panel) were stained with an anti-GFP antibody (right panel, brown) to confirm GFP expression. Bar, 50 μm.

0.08 mm FT(DCM) versus 4.20±0.14 mm MT(DCM), respectively], [LVEF: 77.2±3.1% FT(DCM) versus 73.4± 0.5% MT(DCM), respectively].

3.3. Cardiomyocytes that are derived from transplanted Flk1+ cells express cardiac specific markers

Using immunohistochemistry, we evaluated the differentiation of the transplanted GFP-expressing $Flk1^+$ cells in the hearts of FT(DCM) mice. We detected groups of GFP^+ engrafted cells in DCM hearts within or adjacent to the scar tissue resulting from the injection 4 wks after cell transplantation (Fig. 3I, J) and 10 wks after cell transplantation (Fig. 3K). We confirmed the presence of GFP by immunohistochemistry with an anti-GFP antibody (Fig. 3L). A part of the GFP^+ cells expressed MLC2v, cTn-I, and the sarcomeric marker CH1 (Fig. 4A–C). The GFP^+ cells also expressed Cx43 on their cell membranes (Fig. 4D). Interestingly, these $Cx43^+$ gap junctions were located not only on both ends of the GFP^+ cardiomyocytes, they were also observed on the cell surface. This suggests that the gap junction distribution of engrafted cardiomyocytes may depend on the contact area with other cardiomyocytes. Significantly, the GFP^+ cells expressed ANP at the same low levels as the surrounding host ventricular cells (Fig. 4E). The numbers of engrafted GFP^+ $cTn\text{-}I^+$ cells were 46,403±12,098 cells in a 4 wks FT(DCM) heart and 40,651±14,023 cells in a 10 wks FT(DCM) heart. Although most of the GFP^+ cardiomyocytes were slightly smaller or thinner than the host cardiomyocytes, the strong expression of MLC2v but not ANP indicates that these cells have differentiated into ventricular type cells. These engrafted GFP^+ cells were not stained with skeletal MHC (Supplementary Fig. 1).

We also investigated whether the transplantation resulted in the development of endothelial or hematopoietic $Flk1^+$ cell derivatives. The engrafted GFP^+ cells did not express CD31 (Fig. 4F) and GFP^+ tube-like structures that resemble vessels were not observed. GFP^+ $CD45^+$ cells were scarcely observed in the area of scar (Fig. 4G), suggesting that there is partially differentiation by $Flk1^+$ cells into non-cardiomyocytes upon transplantation. Nevertheless, the overall outcome of the transplantation with these cells is strongly positive since the $Flk1^+$ cells effectively differentiated into ventricular type cardiomyocytes that may well be able to communicate with host cardiomyocytes in the damaged heart environment.

To examine whether transplanted $Flk1^+$ cells have the potential to grow into teratomas, we examined the hearts of transplanted mice. We also examined the effect of ectopically transplanting the $Flk1^+$ cells into the skin of the back, which resulted in subcutaneous lesions, and kidney capsules. While most animals were examined at 4 wks post-transplantation, longer term analyses were performed with five mice that were examined at 10 wks post-transplantation. In the hearts, subcutaneous lesions and kidney capsules, abnormal cell growth around the transplantation area was not observed. We also examined the cell-cycle activity of the engrafted $Flk1^+$ cells in the heart by immunohistochemistry with the anti-Ki-67 antibody. Although the nuclei of almost all undifferentiated Gact4 ES cells and just sorted $Flk1^+$ cells were stained abundantly with the anti-Ki-67 antibody (Supplementary Fig. 2), the nuclei of the engrafted GFP^+ cells that had differentiated in vivo were not stained with this antibody (Fig. 5A). Thus, the engrafted GFP^+ cells that have differentiated from $Flk1^+$ cells in vivo appear to be terminally differentiated.

Unlike $Flk1^+$ cells, $Flk1^-$ cells transplanted into the hearts of DCM mice did not differentiate into cardiomyocytes, and calcification or adipose degeneration were detected in the $Flk1^-$ cell-transplanted hearts (data not shown). This may explain why the transplantation of these cells failed to improve cardiac function. In addition, we detected abnormal cell growth in the hearts of the three of nine $Flk1^-$ cell-transplanted mice (Fig. 5B). Furthermore, we investigated whether transplanted $Flk1^+$ cells fused with host cardiomyocytes. We identified the mouse Y chromosome in Gact4 ES cells via PCR analysis (data not shown) and transplanted these cells into male mice. Although, assessed by FISH analysis, small number of GFP stained nuclei contained two Y chromosomes ($n=9$ in total 158 GFP^+ nuclei; 5.7%), most of GFP stained nuclei contained no more than two Y chromosomes ($n=149$ in total 158 GFP^+ nuclei; 94.3%) (Fig. 5H, I). These results indicated that there was only a small rate of fusion between $Flk1^+$ cells and host cardiomyocytes.

3.4. Cardiomyocytes derived from Flk1+ cells have action potentials

Since we have found that transplanted $Flk1^+$ cells effectively differentiate into ventricular type cells with gap junctions, we next assessed whether these cells have electrical activity. We isolated GFP^+ cardiomyocytes from the $Flk1^+$ cell-transplanted hearts and recorded their action potentials ($n=5$). The shape of the action potentials recorded from these engrafted GFP^+ cells indicates that they are no embryonic or neonatal ventricular type cells, rather, they are adult ventricular type cells [21,22] (Fig. 5C–E), and the resting membrane potentials measured from these engrafted GFP^+ cells (−70.3±±3.9 mV) were equal to those from normal mouse ventricular cells (−71.1±4.4 mV). Moreover, the mean action potential duration at 90% repolarization (APD_{90}) [23] from engrafted GFP^+ cells (116.8±6.6 ms) was not significantly different from normal ventricular cells (113.4±26.5 ms). As expected, day 4-sorted $Flk1^+$ cells had no action potential following electrical stimulation. Furthermore, we recorded electrocardiogram from FT(DCM) mice to investigate whether these differentiated cardiomyocytes produce arrhythmia. We could not detect arrhythmia not only during echocardiography and cardiac catheterization, but also during electrocardiography (Fig. 5J).

3.5. Flk1+ cell-transplantation induced angiogenesis

To assess another mechanism of cardiac improvement, we counted the number of vessels around the $Flk1^+$ cell-injected

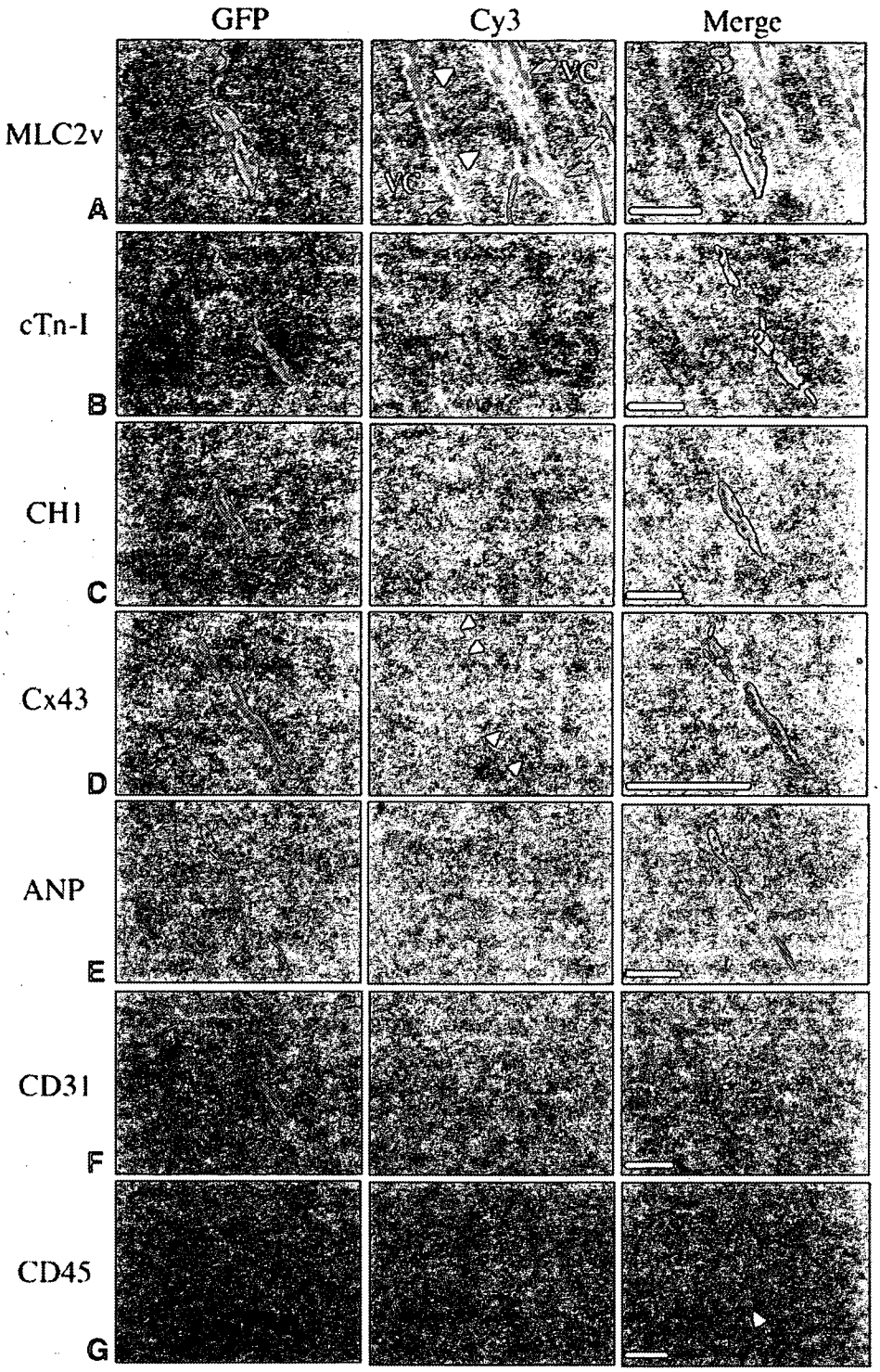

Fig. 4. Engrafted GFP$^+$ cells in the hearts of DCM mice express cardiac-specific markers. (A–G) Engrafted GFP$^+$ cells shown in the left panels (green) were stained for MLC2v (A), cTn-I (B), CH1 (C), Cx43 (D), ANP (E), CD31 (F), and CD45 (G), shown in the middle panels (red). The merged images are shown in the right panels. The white arrowheads in the middle panel of (A) indicate the GFP$^+$ cells surrounded by the host ventricular cells (VC) and the strong but non-specific staining of scar tissue is indicated by the blue arrows. The arrowheads in the middle panel of (D) indicate gap junctions formed between the engrafted cardiomyocytes and endogenous cardiomyocytes. The arrowhead in (G) indicates a CD45$^+$ GFP$^+$ cell. Bar, 50 μm. Nuclei were counterstained with Hoechst 33342 (blue).

or medium-injected sites. Although we could not detect GFP$^+$ CD31$^+$ tubulo-vesicular structures, the number of vessels was significantly higher in the FT(DCM) group than in the MT(DCM) group (Fig. 5F, G). These data indicate that Flk1$^+$ cell-transplantation has a favorable effect on angiogenesis.

4. Discussion

In this report, we demonstrate that Flk1$^+$ cells have a greater potential than Flk1$^-$ cells to differentiate into cardiomyocytes. In addition, Flk1$^+$ cells efficiently differentiated into adult ventricular type cardiomyocytes upon transplantation into DCM model mouse hearts, as shown by immunohistochemistry and electrophysiological examinations. These observations suggest that transplanted Flk1$^+$ cells derived from ES cells may effect a functional improvement in injured hearts.

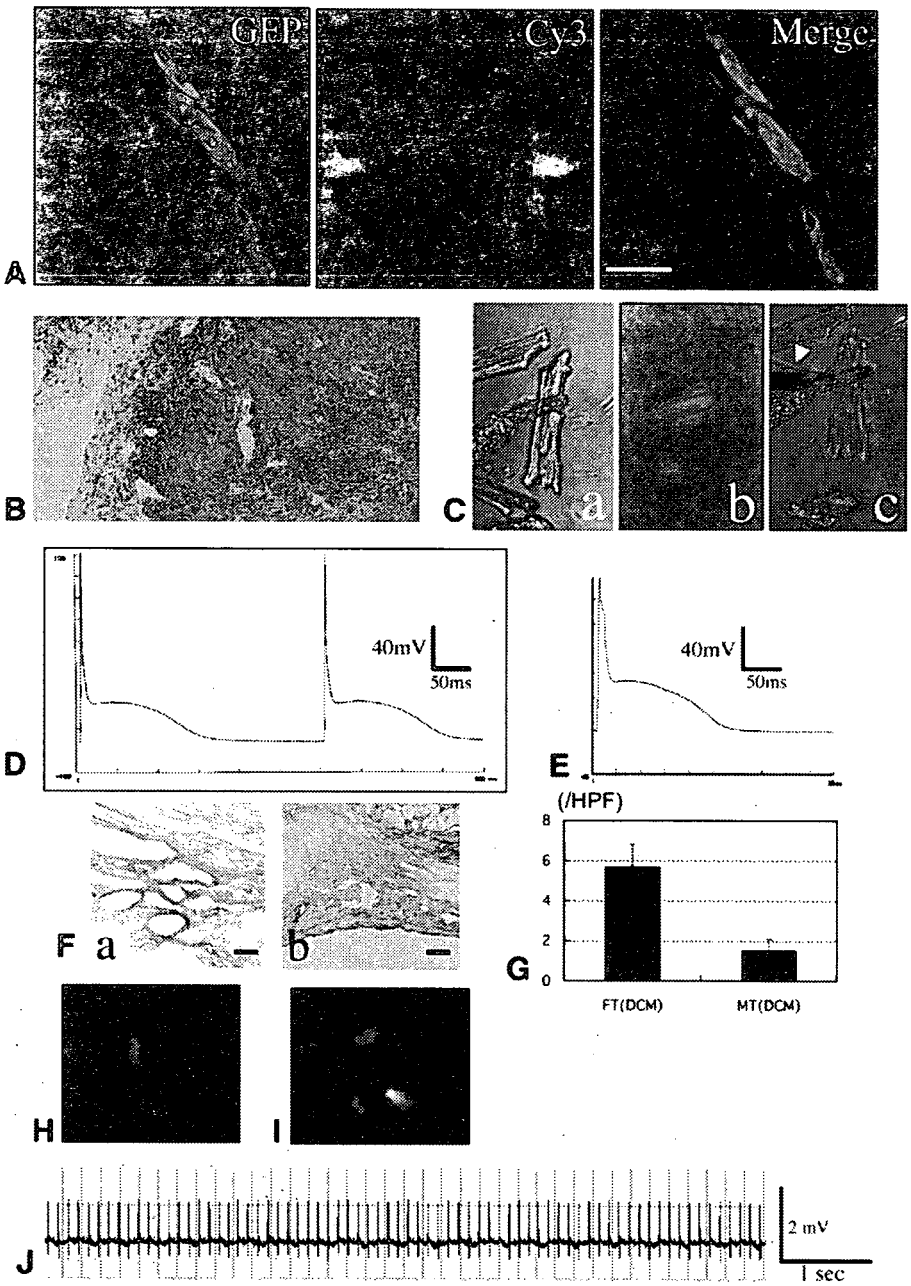

Fig. 5. Engrafted GFP$^+$ cells derived from Flk1$^+$ cells are terminally differentiated and have action potentials, but engrafted cells derived from Flk1$^-$ cells generate abnormal growth. The nuclei of engrafted GFP$^+$ cells derived from Flk1$^+$ cells (green: left panel) do not express Ki-67 (red: middle panel). Right panel: merged images. The nuclei were counterstained with Hoechst 33342 (blue). Bar, 50 μm. (B) Hearts of DCM mice transplanted with Flk1$^-$ cells showed abnormal cell growth. (C–E) Analysis of the action potentials of GFP$^+$ cardiomyocytes in hearts transplanted with Flk1$^+$ cells. The engrafted cardiomyocytes were isolated and identified by fluorescence microscopy (C, panels a and b). The tip of a glass electrode (white arrowhead) was then pressed onto the membrane of a GFP$^+$ cardiomyocyte and its action potential was measured (C, panel c). The GFP$^+$ cardiomyocytes generate ventricular type action potentials following electrical stimulation (D). (E) The action potential of normal mouse cardiomyocytes. (F) The number of CD31$^+$ endothelial cells (brown) stained in the scar area of the FT (DCM) group (left panel a) was significantly greater than those of the MT(DCM) group (right panel b). These endothelial cells were not GFP$^+$ cells. Bar, 10 μm. (G) The number of vessels in scar area of FT(DCM) or MT(DCM) groups was counted. [FT(DCM): left bar, MT(DCM): right bar]. (H) Most of nucleus (blue) containing GFP (green) had only one Y chromosome (red) and did not have more than two. (I) Small number of nucleus (blue) containing GFP (green) had two Y chromosome (red). (J) No arrhythmia was detected from FT(DCM) mice.

Flk1 is a marker of early mesodermal cells, and $Flk1^+$ cells have the potential to differentiate into hematopoietic and endothelial lineages [13,15]. Although cardiomyocytes are also derivatives of mesodermal cells, only a few reports have suggested that expression of Flk1 indicates a commitment to a cardiomyocyte lineage [12,24]. Moreover, while these reports suggest that $Flk1^+$ cells could be cardiac stem/progenitor cells, their functions, differentiation and ability to induce cardiac regeneration in vivo have not been reported previously.

In this report, we found that $Flk1^+$ cells generated regular contractile colonies that expressed cardiac-specific markers much more frequently than $Flk1^-$ cells. Thus, Flk1 is an effective marker for not only hematopoietic and endothelial stem/progenitor cells but also for cardiac stem/progenitor cells expressing Sca-1 and c-kit, which have been reported to be one of the cardiac stem/progenitor cell markers [20]. Although, Nanog and Oct4 were expressed in the population of day 4-sorted $Flk1^+$ cells in our experiments, Yamashita et al. previously reported that day 4-sorted $Flk1^+$ cells lacked the expression of Oct4 [25]. According to this result, the very weak Oct4 and Nanog expressions of day 4-sorted $Flk1^+$ cells in our experiments would be result from the contamination of $Flk1^-$ cells during cell-sorting process. Notably, a previous study by Kouskoff et al. found that the $Flk1^-$ $Brachyury^+$ cell population has a strong potential to differentiate into cardiomyocytes, which seems to contradict our observations. However, this anomaly may be due to the fact that the $Flk1^-$ $Brachyury^+$ cells were harvested on day 3.25 after differentiation in their experiments [26]. In our experiments, we found that some of $Flk1^-$ cells isolated on day 3 converted into $Flk1^+$ cells on day 4 of differentiation. Kattman SJ et al. also reported the difference of cardiac differentiation capacity between day 3.25 differentiated ES cells and day 4.25 differentiated ES cells [27]. Moreover, Kouskoff et al. employed different methods for cell differentiation, which may be another reason for why there are differences between their findings and ours.

Heart cell transplantation using cardiomyopathy models has been the subject of many studies. Candidate cells for heart cell transplantation include fetal cardiomyocytes, skeletal muscle cells, and bone marrow cells. However, routine use of these cell types in the clinic is hampered either by ethical or practical limitations or by the failure of these cells to differentiate in vivo into mature cardiomyocytes. Other, more suitable, candidate cells are adult CS and ES cells, whose transplantation also improves cardiac function in models of cardiomyopathy [10,11]. However, morphological evaluation of the type of cardiomyocytes generated by these cells has not been performed.

We speculated that the best transplantable cell candidate would be one that is as close to the cardiac stem/progenitor level as possible, as these would not only have the capacity to differentiate in vivo into all cardiac lineages, particularly ventricular cells, they would also proliferate well in vitro making it easier to obtain cell numbers sufficient for transplantation. We show here that $Flk1^+$ cells satisfy these requirements, as they have a good potential to proliferate and differentiate into cardiomyocytes upon cell transplantation. Moreover, we found by immunohistochemistry that the engrafted $Flk1^+$ cell derived cardiomyocytes were close to ventricular type cardiomyocytes, as they expressed MLC2v, cTn-I, and CH1, but not ANP. In addition, the electrophysiological response of single engrafted cardiomyocytes, indicated that these cells possessed adult ventricular cell type action potentials, rather than embryonic or neonatal ventricular type potentials [21,22]. Additionally, most of these GFP^+ cardiomyocytes arose as a result of regeneration in host hearts, assessed by FISH analysis. It is not yet clear why these cells spontaneously differentiate into ventricular type cardiomyocytes in vivo, but factors in the damaged ventricle environment may promote their differentiation. Moreover, we found that the engrafted cardiomyocytes have gap junctions on their surfaces. Although we have failed to show the actual direct functional coupling between the GFP^+ cells and endogenous cardiomyocytes as previously reported [28], our results demonstrated that the transplanted cells could not induce any arrhythmias from FT(DCM) mice, which suggest the possibility of functional coupling. Thus, $Flk1^+$ cells transplanted into cardiomyopathic hearts effectively generate into cardiomyocytes that have the potential to communicate with host cardiomyocytes and contribute to contractile function. Although an increased number of vessels in the scar area of the FT(DCM) treatment group was observed more frequently than in the MT(DCM) group, we could not detect GFP^+ $CD31^+$ cells forming vascular structures. This may be due to the fact that we did not use an ischemic animal model in which angiogenesis from $Flk1^+$ cells would be strongly induced.

A major concern about using ES cells in clinical settings is that they may generate teratomas [29]. However, in this study, we did not find abnormal cell growth in the hearts of any of the FT(DCM) mice. We also conducted a longer term study of this problem by transplanting $Flk1^+$ cells into an additional five mice and sacrificing them ten weeks post-transplantation. No abnormal cell growths were observed. Moreover, we could not detect Ki-67 in the nuclei of engrafted cells at 4 wks post-transplantation, which suggests that these cells have terminally differentiated. In contrast, the transplantation of $Flk1^-$ cells led to tumors in the hearts of three of nine mice. Thus, unlike the heterogeneous and undifferentiated $Flk1^-$ cells, which expressed high levels of Nanog and Oct4, $Flk1^+$ cells sorted on day 4 of ES cell differentiation lack the potential to induce abnormal cell growth and are therefore likely to be relatively safer cell transplantation candidates than $Flk1^-$ cells.

$Flk1^+$ cell-transplanted DCM mice were examined by echocardiography and cardiac catheterization to measure the effect of the transplantation on cardiac function. The cardiac function values determined by these methods revealed that the transplanted $Flk1^+$ cells favorably influenced the systolic and diastolic function of the left ventricle. Although we cannot declare the engrafted GFP^+ $cTn\text{-}I^+$ cell number is

sufficient for the recovery of cardiac function, this recovery in the transplanted DCM mice is likely to be partly due to the cooperative contractile function of the cardiomyocytes derived from the $Flk1^+$ cells and angiogenesis induced by $Flk1^+$ cell-transplantation. However, the improved cardiac function could be the result of other mechanisms that arise from the $Flk1^+$ cell transplantation. These possibilities will be investigated in future experiments.

In conclusion, by using a simple cell sorting method, we were able to collect numerous cardiac stem/progenitor cells that have the potential to differentiate into cardiomyocytes both in vitro and in vivo from differentiating ES cells. Furthermore, the cardiomyocytes generated by these stem/progenitor cells improve cardiac function in a cardiomyopathy mouse model. However, we have not yet been able to isolate committed cardiac stem/progenitor cells that exclusively differentiate into cardiomyocytes. The search for these cells will be the subject of future studies.

Acknowledgements

We thank Dr. Ogawa for kindly providing the Gact4 ES cell line, Dr. Kodama for generously providing the OP-9 stromal cell line, and Dr. Shioya for valuable advice about cell isolation method.

This study was supported by the Program for Promotion of Fundamental Studies in Health Science of the National Institute of Biomedical Innovation (NIBIO) (03-2) and Research of Japan, and by a Grant-in-Aid for Creative Scientific Research (13GS0009).

Appendix A. Supplementary data

Supplementary data associated with this article can be found, in the online version, at doi:10.1016/j.cardiores.2007.05.013.

References

[1] Etoch SW, Koenig SC, Laureano MA, Cerrito P, Gray LA, Dowling RD. Results after partial left ventriculectomy versus heart transplantation for idiopathic cardiomyopathy. J Thorac Cardiovasc Surg 1999;117: 952–9.

[2] Reinecke H, Zhang M, Bartosek T, Murry CE. Survival, integration, and differentiation of cardiomyocyte grafts: a study in normal and injured rat hearts. Circulation 1999;100:193–202.

[3] Menasche P, Hagege AA, Scorsin M, Pouzet B, Desnos M, Duboc D, et al. Myoblast transplantation for heart failure. Lancet 2001;357:279–80.

[4] Scorsin M, Hagege A, Vilquin JT, Fiszman M, Marotte F, Samuel JL, et al. Comparison of the effects of fetal cardiomyocyte and skeletal myoblast transplantation on postinfarction left ventricular function. J Thorac Cardiovasc Surg 2000;119:1169–75.

[5] Gutstein DE, Morley GE, Tamaddon H, Vaidya D, Schneider MD, Chen J, et al. Conduction slowing and sudden arrhythmic death in mice with cardiac-restricted inactivation of Connexin43. Circ Res 2001;88: 333–9.

[6] Kocher AA, Schuster MD, Szabolcs MJ, Takuma S, Burkhoff D, Wang J, et al. Neovascularization of ischemic myocardium by human bone-marrow-derived angioblasts prevents cardiomyocyte apoptosis, reduces remodeling and improves cardiac function. Nat Med 2001;7:430–6.

[7] Murry CE, Soonpaa MH, Reinecke H, Nakajima H, Nakajima HO, Rubart M, et al. Haematopoietic stem cells do not transdifferentiate into cardiac myocytes in myocardial infarcts. Nature 2004;428: 664–8.

[8] Fijnvandraat AC, van Ginneken AC, de Boer PA, Ruijter JM, Christoffels VM, Moorman AF, et al. Cardiomyocytes derived from embryonic stem cells resemble cardiomyocytes of the embryonic heart tube. Cardiovasc Res 2003;58:399–409.

[9] Hidaka K, Lee JK, Kim HS, Ihm CH, Iio A, Ogawa M, et al. Chamber-specific differentiation of Nkx2.5-positive cardiac precursor cells from murine embryonic stem cells. FASEB J 2003;17:740–2.

[10] Beltrami AP, Barlucchi L, Torella D, Baker M, Limana F, Chimenti S, et al. Adult cardiac stem cells are multipotent and support myocardial regeneration. Cell 2003;114:763–76.

[11] Min JY, Yang Y, Converso KL, Liu L, Huang Q, Morgan JP, et al. Transplantation of embryonic stem cells improves cardiac function in postinfarcted rats. J Appl Physiol 2002;92:288–96.

[12] Iida M, Heike T, Yoshimoto M, Baba S, Doi H, Nakahata T. Identification of cardiac stem cells with FLK1, CD31, and VE-cadherin expression during embryonic stem cell differentiation. FASEB J 2005;19:371–8.

[13] Nishikawa SI, Nishikawa S, Hirashima M, Matsuyoshi N, Kodama H. Progressive lineage analysis by cell sorting and culture identifies FLK1+VE-cadherin+cells at a diverging point of endothelial and hemopoietic lineages. Development 1998;125:1747–57.

[14] Ogawa M, Kizumoto M, Nishikawa S, Fujimoto T, Kodama H, Nishikawa SI. Expression of alpha4-integrin defines the earliest precursor of hematopoietic cell lineage diverged from endothelial cells. Blood 1999;93:1168–77.

[15] Hirashima M, Kataoka H, Nishikawa S, Matsuyoshi N, Nishikawa S. Maturation of embryonic stem cells into endothelial cells in an in vitro model of vasculogenesis. Blood 1999;93:1253–63.

[16] Umeda K, Heike T, Yoshimoto M, Shiota M, Suemori H, Luo HY, et al. Development of primitive and definitive hematopoiesis from nonhuman primate embryonic stem cells in vitro. Development 2004;131: 1869–79.

[17] Nishio R, Sasayama S, Matsumori A. Left ventricular pressure–volume relationship in a murine model of congestive heart failure due to acute viral myocarditis. J Am Coll Cardiol 2002;40:1506–14.

[18] Yoshimoto M, Chang H, Shiota M, Kobayashi H, Umeda K, Kawakami A, et al. Two different roles of purified CD45+c-Kit+Sca-1+Lin-cells after transplantation in muscles. Stem Cells 2005;23: 610–8.

[19] Kuratomi S, Matsuoka S, Sarai N, Powell T, Noma A. Involvement of Ca2+ buffering and Na+/Ca2+ exchange in the positive staircase of contraction in guinea-pig ventricular myocytes. Pflugers Arch 2003;446: 347–55.

[20] Jackson KA, Majka SM, Wang H, Pocius J, Hartley CJ, Majesky MW, et al. Regeneration of ischemic cardiac muscle and vascular endothelium by adult stem cells. J Clin Invest 2001;107:1395–402.

[21] Wang L, Feng ZP, Kondo CS, Sheldon RS, Duff HJ. Developmental changes in the delayed rectifier K+ channels in mouse heart. Circ Res 1996;79:79–85.

[22] Wobus AM, Kleppisch T, Maltsev V, Hescheler J. Cardiomyocyte-like cells differentiated in vitro from embryonic carcinoma cells P19 are characterized by functional expression of adrenoceptors and Ca2+ channels. In Vitro Cell Dev Biol Anim 1994;30A:425–34.

[23] Heath BM, Xia J, Dong E, An RH, Brooks A, Liang C, et al. Overexpression of nerve growth factor in the heart alters ion channel activity and beta-adrenergic signalling in an adult transgenic mouse. J Physiol 1998;512:779–91.

[24] Motoike T, Markham DW, Rossant J, Sato TN. Evidence for novel fate of Flk1+ progenitor: contribution to muscle lineage. Genesis 2003;35: 153–9.

[25] Yamashita JK, Takano M, Hiraoka-Kanie M, Shimizu C, Peishi Y, Yanagi K, et al. Prospective identification of cardiac progenitors by a novel single cell-based cardiomyocyte induction. FASEB J 2005;19 (11):1534–6.

[26] Kouskoff V, Lacaud G, Schwantz S, Fehling HJ, Keller G. Sequential development of hematopoietic and cardiac mesoderm during embryonic stem cell differentiation. Proc Natl Acad Sci U S A 2005;102:13170–5.

[27] Kattman SJ, Huber TL, Keller GM. Multipotent Flk1-1+ cardiovascular progenitor cells give rise to cardiomyocyte, endothelial, and vascular smooth muscle lineages. Dev Cell 2006;11(5):723–32.

[28] Rubart M, Pasumarthi KB, Nakajima H, Soonpaa MH, Nakajima HO, Field LJ. Physiological coupling of donor and host cardiomyocytes after cellular transplantation. Circ Res 2003;92(11):1176–8.

[29] Swijnenburg RJ, Tanaka M, Vogel H, Baker J, Kofidis T, Gunawan F, et al. Embryonic stem cell immunogenicity increases upon differentiation after transplantation into ischemic myocardium. Circulation 2005;112:I166–72.

EXPERIMENTAL CELL RESEARCH 313 (2007) 1008–1023

available at www.sciencedirect.com

ScienceDirect

www.elsevier.com/locate/yexcr

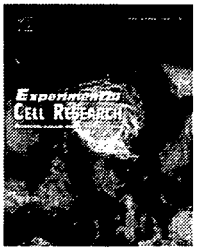

Research Article

Isolation and characterization of bone marrow-derived mesenchymal progenitor cells with myogenic and neuronal properties

*Mitsutaka Shiota, Toshio Heike, Munetada Haruyama, Shiro Baba, Atsunori Tsuchiya, Hisanori Fujino, Hirohiko Kobayashi, Takeo Kato, Katsutsugu Umeda, Momoko Yoshimoto, Tatsutoshi Nakahata**

Department of Pediatrics, Graduate School of Medicine, Kyoto University, 54 Kawahara-cho, Shogoin, Sakyo-ku, Kyoto 606-8507, Japan

ARTICLE INFORMATION

Article Chronology:
Received 25 May 2006
Revised version received
21 November 2006
Accepted 27 December 2006
Available online 8 January 2007

Keywords:
Multipotent spheres
Murine bone marrow
Mesenchymal stem cells
Cardiomyocytes
Neurons
Skeletal myoblasts
Acute myocardial infarction

ABSTRACT

Sphere formation has been utilized as a way to isolate multipotent stem/progenitor cells from various tissues. However, very few studies on bone marrow-derived spheres have been published and assessed their multipotentiality. In this study, multipotent marrow cell populations were isolated using a three-step method. First, after elimination of hematopoietic cells, murine marrow-derived adherent cells were cultured in plastic dishes until small cells gradually appeared and multiplied. Cells were then cultured under non-adherent conditions and formed spheres that were immunopositive for a neural precursor marker, nestin. RT-PCR analysis also revealed that the spheres were positive for nestin in addition to PPARγ, osf2, SOX9, and myoD, which are markers of precursors of adipocytic, osteoblastic, chondrocytic, and skeletal myeloblastic lineages, respectively. Finally, spheres were dissociated into single cells and expanded in adherent cultures. Under appropriate induction conditions, the sphere-derived cells acquired the phenotypic properties in vitro of neurons, skeletal myoblasts, and beating cardiomyocytes, as well as adipocytes, osteoblasts, and chondrocytes. Next, sphere-derived cells were transplanted into murine myocardial infarction models. One month later, they had become engrafted as cardiomyocytes, and cardiac catheterization showed significant functional improvements. Thus, sphere-derived cells represent a new approach to enhance the multi-differentiation potential of murine bone marrow.

Introduction

Human mesenchymal stem cells (MSCs), originally discovered by Friedenstein et al. [1] in 1976, can be isolated with relative ease from bone marrow utilizing plastic adherent methods [1,2]. MSCs can differentiate into three classical mesenchymal cell types (adipocytes, osteoblasts, and chondrocytes) [2]. Recently, they were also reported to be capable of differentiating into other lineages including neurons [3] and cardiomyocytes [4]. Based on this evidence, several clinical trials using human MSCs have been aimed at treating osteogenesis imperfecta [5], myocardial infarction [6], and so on. In addition, stem/progenitor cells with greater multipotentiality have been successfully isolated and expanded from human bone marrow

* *Corresponding author.* Fax: +81 75 752 2361.
E-mail address: tnakaha@kuhp.kyoto-u.ac.jp (T. Nakahata).

0014-4827/$ – see front matter © 2007 Elsevier Inc. All rights reserved.
doi:10.1016/j.yexcr.2006.12.017

stroma in the hope of developing treatments for a number of human diseases. These multipotent stem/progenitor cells include human marrow-isolated adult multi-lineage inducible (MIAMI) cells [7], multipotent adult progenitor cells (MAPCs) [8], and human BM-derived multipotent stem cells (hBMSCs) [9].

Several investigators have urged that cautions be exercised in therapeutic applications of such stem/progenitor cells until we have acquired a better understanding of their fundamental properties. Referring to MSCs, Javazon et al. [10] proposed that therapeutic trials with MSCs remain limited until the *in vivo* biology of MSCs and the therapeutic potential of passaged MSCs are better understood. For this purpose, *in vitro* and *in vivo* characterization of the biology of MSCs in non-human animals, such as mice, is necessary.

In contrast to human MSCs, easy and reproducible methods to enrich and expand murine MSCs have not yet been established. The isolation of murine MSCs by standard techniques involving adherence to plastic is difficult because of the possibility of contamination by macrophages, endothelial cells, lymphocytes, and smooth muscle cells both in early marrow populations and in passaged cultures [11]. Such unwanted cells often prevent the growth of MSCs. In addition, long-term *in vitro* culture of MSCs is difficult due to their tendency to lose progressively their capacity to proliferate and differentiate [10,12].

To overcome these problems, several groups have reported new protocols for isolating murine MSCs or marrow stem/progenitor cells. Most of the cells isolated, however, show differentiation potential into only two or three classical mesenchymal lineages [13–15]. The exception is murine MAPCs, which are difficult to isolate; many researchers including our own group, have failed to establish fully multipotent MAPCs. Therefore, it is necessary to establish more standardized culturing protocols for murine MSCs or marrow-derived multipotent stem/progenitor cells.

Sphere formation has been reported to constitute a step for the establishment of multipotent stem/progenitor cells from various tissues such as skin [16], mammary gland [17], and hepatocyte [18]. However, only a few studies identified bone marrow-derived spheres [3,19] that can differentiate into neurons and/or glial cells, and none of these reports addressed multipotentiality.

Here we report a method enabling isolation of murine bone marrow cells with greater multipotency than classical mesenchymal lineages. We assess the multi-differentiation potential in vitro of a cell population obtained by sphere formation, as well as their in vivo differentiation and functional capabilities in a model of acute myocardial infarction.

Materials and methods

Isolation and culture of sphere-derived cells from murine bone marrow

Isolation

Female 4- to 6-week-old C3H/He mice were purchased from Charles River Laboratories (Kyoto, Japan). All experiments in this study were performed in accordance with the Animal Protection Guidelines of Kyoto University. Bone marrow cells (BMCs) were obtained from five mice for each experiment as previously described [20]. Whole BMCs were suspended in Iscove's modified Dulbecco's medium (IMDM; Sigma, St. Louis, MO) supplemented with 20% heat-inactivated fetal calf serum (FCS; Gibco BRL, Grand Island, NY, Lot No: US172777), penicillin (100 IU/ml), and streptomycin (100 μg/ml) (complete medium).

To remove differentiated hematopoietic cells, lineage$^+$ cells were depleted from whole BMCs by means of immunomagnetic separation with Dynabeads according to the manufacturer's protocol. Briefly, BMCs were stained with primary rat-anti-mouse antibodies, namely anti-CD4, CD8, CD11b, CD45R/B220, Gr-1, and Ter119 (all purchased from PharMingen, San Jose, CA). After centrifugation of the labeled cells, Dynabeads M-450 Sheep anti-Rat IgG (Dynal Biotech, Oslo, Norway) were added at a concentration of 10 beads per cell. The mixture was placed on a Dynal Magnetic Particle Concentrator (Dynal Biotech) for one minute and the supernatant containing the lineage-depleted BMCs was collected.

Immunodepleted BMCs were resuspended in 10 ml of complete medium and plated on a 59-cm^2 Primaria™ tissue culture dish (BD Falcon, Lincoln Park, NY). Cells were cultured in a humidified incubator containing 5% CO_2 and 5% O_2 at 37 °C. After 24 h, non-adherent cells were removed by washing with phosphate-buffered saline (PBS) and fresh complete medium was added. Thereafter, the medium was changed twice a week for 3 to 4 weeks, when cells first reached 70–80% confluency. Then adherent cells were detached with Pronase (Kyokuto Seiyaku, Tokyo, Japan) for 30 min at 37 °C. Only easily detached cells were plated on a 59-cm^2 standard tissue culture dish (BD Falcon) (first passage). After the first passage, cells were cultured under similar conditions, except that the split ratio was set to 1:2. After an additional 5–7 passages, cells were detached at a lower cell density (40–50% confluence). The same conditions were used for subsequent cultures after small round and oval-shaped cells had become predominant at the sixth to eighth passage.

Sphere formation and culture expansion

A total of 1×10^5 cells were suspended in complete medium in each well of a 6-well ultra low attachment plate (Corning Inc., Corning, NY). Cells were cultured without changing the medium and rotated gently every 6 h. The spheres gradually increased in size and 7 days after suspension were picked and dissociated mechanically by gentle pipetting. Dissociated cells were cultured in complete medium on standard tissue culture dishes and the medium was changed twice a week. After reaching 40–50% confluency, cells were detached with Pronase and replated at a 1:4 dilution. Sphere-derived cells were harvested for the experiments described below when one well of the original culture contained more than 1×10^7 cells.

Flow cytometric analysis of sphere-derived cells

Sphere-derived cells were analyzed by FACS Caliber (Becton Dickinson, San Jose, CA) as previously reported [21]. The following primary antibodies were used: fluorescein isothiocyanate (FITC)-conjugated CD29, CD49d, CD90.2 (Thy1.2), and H-2K^k antibodies; phycoerythrin (PE)-conjugated Sca-1, CD13, CD31, CD34, CD49f, Flk-1, Gr-1, and Ter119 antibodies; (APC)-

conjugated CD45, CD45R/B220, and CD117 (c-kit) antibodies; biotinylated CD4, CD8a, CD11b/Mac1, CD44, CD144 (VE-cadherin), and I-A^k antibodies; and purified rat anti-mouse CD105 antibody. In some experiments, streptavidin-FITC, PE, and APC conjugates and APC-conjugated goat anti-rat antibodies were used as secondary antibodies. Isotype control experiments were run in parallel using the same concentration of each antibody. All antibodies were purchased from PharMingen. At least 10,000 events were collected and analyzed with Cell Quest (BD Biosciences Clontech, Palo Alto, CA) software.

In vitro phenotypic acquisition of multiple lineages by sphere-derived cells

Adipogenic differentiation

Adipogenic property was induced as previously described [2], except for the addition of 3-isobutyl-1-methylxanthine (IBMX). Briefly, confluent sphere-derived cells were cultured in α-minimum essential medium (α-MEM) supplemented with 10% FCS, 0.5 mM IBMX, 10 μg/ml insulin, and 1 μM dexamethasone (all from Sigma) for 21 days.

For Oil-red O staining, cells were fixed with 4% paraformaldehyde (PFA) and stained for 15 min in fresh Oil-Red O working solution (three volumes of 0.5% Oil Red O (Sigma) in isopropyl alcohol plus two volumes distilled water).

Osteogenic differentiation

To acquire the osteogenic property, confluent sphere-derived cells were cultured as described [2]. Briefly, cells were cultured in α-MEM with 10% FCS, 10 mM β-glycerophosphate, 50 μg/ml ascorbic acid 2-phosphate, and 10 nM dexamethasone (all from Sigma) for 28 days.

For alkaline phosphatase staining, cells were fixed with 4% PFA, washed in 10 mM Tris buffer (pH 7.5, Nakalai Tesque, Inc., Kyoto, Japan), and stained with alkaline phosphatase solution (5 mg naphthol AS-MX phosphate [Sigma] and 30 mg fast blue BB salt [Sigma] in 0.2 M Tris buffer [pH 8.5]) at room temperature (RT) for 30 min.

Mineralized matrix was evaluated by von Kossa staining. Cells were fixed with 4% PFA and overlaid with a 5% silver nitrate (Sigma) solution in the absence of light at RT for 30 min. Cells were then exposed to sunlight for 5 min and excess silver staining was removed by washing with a 5% sodium thiosulfate (Nakalai Tesque) solution.

Chondrogenic differentiation

The chondrogenic phenotype was acquired as previously described [22]. Briefly, confluent sphere-derived cells were cultured in Dulbecco's modified Eagles medium nutrient mixture F-12 HAM (Sigma) containing 5% FCS, 10 μg/ml transferrin, 10 μg/ml insulin, and 3×10^{-8} M sodium selenite (all from Sigma) for 28 days.

For Alcian blue staining, the cells were fixed with methanol at −20 °C for 5 min and stained with 0.1% Alcian blue (0.1N HCl, Sigma) overnight.

Neuronal differentiation

To acquire the neuronal property, sphere-derived cells were treated as previously described [23] with some modifications. Briefly, cells were plated at a cell density of 1×10^4 cells/cm^2 on gelatin-coated dishes in neurobasal medium (Gibco BRL) with B27 Supplement (50×, Invitrogen, Carlsbad, CA), 20 ng/ml EGF (Sigma), and 10 ng/ml bFGF (Sigma) for 7 days, followed by culture in neurobasal medium with 0.5 μM retinoic acid (Sigma) and 20 ng/ml β-NGF (Sigma) for 5 days.

For immunofluorescence, cells were fixed in 4% PFA, permeabilized with 0.2% Triton X-100 in PBS at 4 °C for 30 min, blocked with 0.5% casein and 5% normal goat serum in PBS at 4 °C for 30 min, and sequentially incubated with anti-nestin (1:200; Chemicon International Inc., Temecula, CA) or β-tubulin III (1:500, Sigma) antibodies at 4 °C overnight, followed by incubation with secondary antibodies coupled with cytochrome 3 (Cy3, 1:200, Jackson Immunoresearch, West Grove, PA) at RT for 1 h. Between each step, cells were washed three times with 0.1% Tween in PBS. Fluorescence was detected and photographed with an AxioCam photomicroscope (Carl Zeiss Vision GmbH, Hallbergmoos, Germany). The immunofluorescent staining of a single sphere was performed as previously described [24].

Skeletal myoblast and cardiomyocyte differentiation

Skeletal myoblast and cardiomyocyte phenotypes were induced as described [4,25]. Briefly, confluent sphere-derived cells were first cultured in IMDM with 2% FCS and 0.5 μM 5-aza-2′-deoxycytidine (Sigma) for 24 h and then in IMDM with 10% FCS for 28 days.

Immunohistochemistry was performed as described [26]. Primary antibodies used in this study were anti-desmin (1:20 dilution, Sigma), skeletal myosin (1:50, Zymed Laboratories Inc., South San Francisco, CA), myosin light chain 2v (MLC2v, 1:100, Alexis Biochemicals Inc., Montreal, Canada) and atrial natriuretic peptide (ANP, 1:100; Protos Biotech, NY). Cells were stained with secondary antibodies coupled with horseradish peroxidase and reactions were visualized by adding 3, 3-diaminobenzidine (DAB, Vector Laboratories, Inc., Burlingame, CA).

The percentage of phenotypically differentiated cells in each lineage

After differentiation as described previously, the percentage of each phenotype was calculated in five randomly-selected fields (×200 magnification) by counting the number of nucleated cells by Hoechst33342 nuclear staining (1:2000, Molecular Probes, Leiden, The Netherlands) together with one of following stainings; Oil red O staining, alkaline phosphatase staining, Alcian blue staining, immunofluorescent staining for β-tubulin III, and DAB staining of skeletal myosin and MLC2v as described above. For cardiomyocytic differentiation, all the cardiomyocytes were counted in one 10-cm dish.

RNA isolation and RT-PCR analysis

RT-PCR was undertaken as previously described [27] with the oligonucleotide primers listed in Table 1. For semi-quantitative comparisons, samples were normalized by dilution to yield equivalent signals for HPRT. Total RNAs from limb buds of murine embryos at 16.5 days post coitum (16.5 dpc) were used as positive controls for the chondrogenic lineage and those isolated at 18.5 dpc were used for adipogenic, osteogenic, and skeletal muscle lineages. Those

Table 1 – Primers used for RT-PCR

Primer	Sequence	Product
Peroxisome proliferator activated receptor γ	S: 5′-ACCAAGTGACTCTGCTCAAG-3′ A: 5′-GGCTTCACGTTCAGCAAGCC-3′	279 bp
Adipocyte P2	S: 5′-TGTGATGCCTTTGTGGGAACC-3′ A: 5′-CGTCTGCGGTGATTTCATCTG-3′	221 bp
Osteoblastic specific factor-2	S: 5′-GAGGGCACAAGTTCTATCTGGAA-3′ A: 5′-CTACAACCTTGAAGGCCACG-3′	491 bp
Osteocalcin	S: 5′-TCTGACAAAGCCTTCATGTC-3′ A: 5′-AAATAGTGATACCGTAGATGCG-3′	201 bp
SOX9	S: 5′-GAAGCTGGCAGACCAGTACC-3′ A: 5′-CTGCTCAGTTCACCGATGTC-3′	479 bp
Collagen type II	S: 5′-GTGAGCCATGATCCGC-3′ A: 5′-GACCAGGATTTCCAGG-3′	174 bp
Nestin	S: 5′-GGATACAGCTTTATTCAAGG-3′ A: 5′-CAGCCGCTGAAGTTCACTCT-3′	481 bp
Neurofilament M	S: 5′-CCTCTGTACACACACCGACA-3′ A: 5′-TAGCCTCAGGAGACTTCACG-3′	273 bp
MyoD	S: 5′-ATCCGCTACATCGAAGGTCT-3′ A: 5′-CTCTGGTGGTGCATCTGCCA-3′	371 bp
Myogenin	S: 5′-CAGTACATTGAGCGCCTACA-3′ A: 5′-ACATATCCTCCACCGTGATG-3′	264 bp
Desmin	S: 5′-ATCTCTGAGGCTGAAGAATGG-3′ A: 5′-GAGCAGAGAAGGTCTGGATAG-3′	414 bp
Myosin light chain 2v	S: 5′-GCCAAGAAGCGGATAGAAGG-3′ A: 5′-CTGTGGTTCAGGGCTCAGTC-3′	502 bp
Myosin light chain 2a	S: 5′-CAGACCTGAAGGAGACCT-3′ A: 5′-GTCAGCGTAAACAGTTGC-3′	278 bp
Nkx2.5	S: 5′-CCAAGTGCTCTCCTGCTTTC-3′ A: 5′-GTAGCCATAGGCATTGAGAC-3′	503 bp
Oct-4	S: 5′-GGCGTTCTCTTTGGAAAGGTG-3′ A: 5′-CTCGAACCACATCCTTCTCT-3′	315 bp
Rex1	S: 5′-AAAGTGAGATTAGCCCCGAG-3′ A: 5′-TCCCATCCCCTTCAATAGCA-3′	933 bp
Brachyury	S: 5′-TTTCTTGGAAAAGCGGTGGC-3′ A: 5′-CCCGTTCACATATTTCCAGCG-3′	411 bp
HPRT	S: 5′-GCTGGTGAAAAGGACCTCT-3′ A: 5′-CACAGGACTAGAACACCTGC-3′	251 bp

from whole brain of 18.5 dpc murine embryos and heart tissue from a 4-week-old mouse were used as positive controls for neuronal and cardiomyocytic lineages, respectively. Undifferentiated murine ES cells were used for Oct-4 and Rex1, and cells from 7.5 dpc mouse embryos were used for Brachyury.

Retroviral transduction of eGFP into sphere-derived cells

Retroviral supernatants were produced by calcium phosphate-mediated transfection [28]. Briefly, phoenix cells, generously provided by Dr. G. Nolan, were transfected with a retroviral plasmid, pMSCV (murine stem cell virus)-EGFP (enhanced green fluorescent protein), which was kindly provided by Dr. R. Nishikomori, in DMEM/10%FCS for 8 h after which the medium was replaced. Two days after transfection, sphere-derived cells were incubated with the retroviral supernatant and 4 μg/ml polybrene (Sigma) and centrifuged at 1200×*g*, RT for 90 min. The supernatants containing the retrovirus were harvested after 20 h and the cells were incubated for another 2 days. Transduction efficiency was analyzed by FACS Caliber and GFP^+ cells were collected by cell sorting on FACS Vantage (Becton Dickinson).

In vivo engraftment of sphere-derived cells: acute myocardial infarction (AMI) model

Male 10-week-old C3H/He mice were endotracheally intubated, anesthetized with 1% isoflurane gas, and ventilated by ventilators before ligating their left anterior descending coronary arteries. PBS (10 μl) containing 1×10^6 GFP-transduced sphere-derived cells, which were pretreated with 0.5 μM 5-aza-2′-deoxycytidine for 24 h, were directly injected with a 27-gauge needle into one site of the peri-infarcted area of the left ventricular free wall, and the chests were closed aseptically. Non-injected infarcted mice (AMI group) or infarcted mice injected with 10 μl PBS only (PBS group) and untreated normal mice served as controls (five mice for each group).

Four weeks after surgery, cardiac catheterization was performed to assess left ventricle (LV) function. Mice were anesthetized and their right carotid arteries were cannulated with 1.4-Fr micromanometer-tipped catheters (Millar Instruments Inc., Houston, TX) connected to pressure transducers (model TCB-500, Millar Instruments Inc.). Cardiac pressures were monitored and recorded on chart-strip recorders (Thermal Array Recorder, model RTA-1100M; Nihon Kohden, Tokyo, Japan). The maximum rate of LV

systolic pressure (+dP/dt), the minimum rate of LV diastolic pressure (−dP/dt), and LV end-diastolic pressure (LVEDP) were calculated from the inclination of the recorded pressure curves.

Subsequent immunohistochemistry was performed as described [26]. Implanted hearts were perfused with PBS and fixed with 4% PFA. After gradual equilibration in 15%, 20%, and 30% sucrose over 2 days, tissues were embedded in Optimal Cutting Temperature Compound (Ted Pella Inc., Redding, CA) and quickly frozen in liquid nitrogen. Cryostat sections (7 μm thick) were permeabilized and background staining due to endogenous murine immunoglobulins was eliminated using the Vector M.O.M. immunodetection kit (Vector Laboratories) according to the manufacturer's protocol. Sections were then stained with primary antibodies against cardiac troponin I (1:50, Santa Cruz Biotechnology Inc., Santa Cruz, CA), sarcomeric tropomyosin (1:100, Sigma), and CD31 (1:100, PharMingen) and were visualized with secondary antibodies conjugated to Cy3. For nuclear staining, cells were stained with Hoechst33342 at RT for one minute. Images were taken with fluorescent (Olympus, Tokyo, Japan) or confocal (Leica, Heerbrugg, Switzerland) stereomicroscopes. A total of 10 visual fields, where a cross section of capillaries was clearly visible, were randomly selected in the peri-infarct area, and the numbers of CD31-positive vessels were counted under ×200 magnification ($n=5$ per group).

Statistical analysis

Results are presented as means±SD. Significant differences between two measurements were determined with the Student's t-test. P values <0.01 were considered significant.

Results

Isolation of marrow-derived cells forming floating spheres

Fig. 1 shows a schematic representation of the isolation of multipotent marrow cells using sphere formation. Cells grown in media containing the FCS had almost no ability to form hematopoietic colonies in the *in vitro* colony assays. To remove differentiated hematopoietic cells and prevent their excess growth, mature hematopoietic cells were depleted by immunomagnetic separation with Dynabeads. After depletion, the total number of cells was reduced from 4.2±0.85 (2.8 to 5.8, $n=5$)×10^8 BMCs to 3.3±1.5 (1.0 to 5.7, $n=5$)×10^6 BMCs. Since lineage$^-$ cells did not form symmetrical spheres in suspension cultures at this stage ($n=10$), we expanded them first in adherent cultures before sphere formation.

When lineage$^-$ cells were plated on standard tissue culture dishes, adherent cells did not proliferate to form colonies. Thus, we plated them on Primaria™ tissue culture dishes, which supported attachment and spreading of several cell types. After the medium was changed at 24 h, at most one adherent fibroblast-like cell per high-power field remained, and even on day 7, adherent cells appeared in the form of individual cells or clusters consisting of a few cells. However, adherent cells formed large heterogeneous colonies after 3–4 weeks when they were replated. After the first passage, adherent cells proliferated on standard tissue culture dishes, and after the sixth to eighth passage, small, round, and oval cells gradually increased and became predominant. Cells at this stage (non-spheres) were then cultured under their respective specialized differentiation conditions. In contrast to the three classical mesenchymal lineages, phenotypic

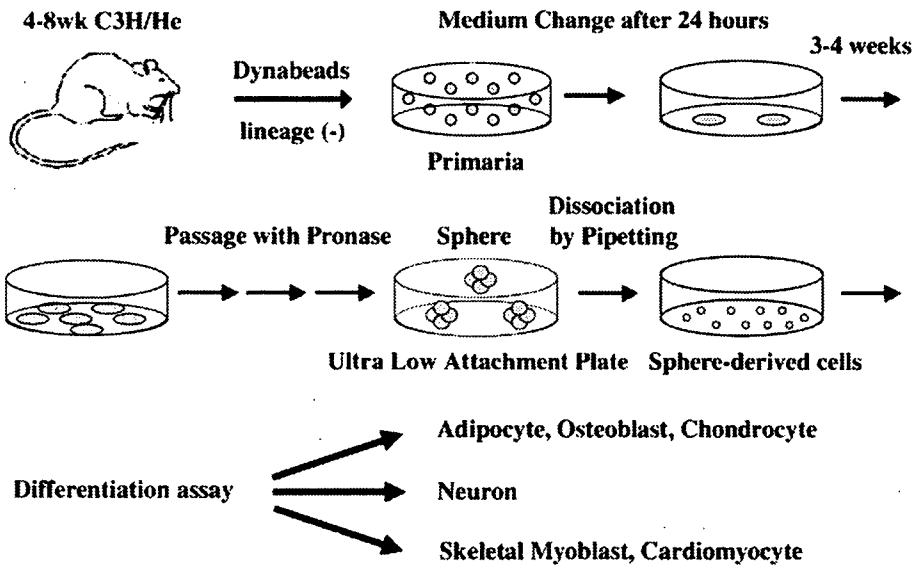

Fig. 1 – Schematic representation of the protocol to generate multipotent marrow cell populations. Lineage$^-$ cells were selected from bone marrow cells of 4- to 6-week-old C3H/He mice using Dynabeads, plated on a Primaria™ tissue culture dish in IMDM supplemented with 20% FCS, and incubated in 5% CO_2 and 5% O_2. After 24 h, the medium was replaced and adherent cells were subcultured. After small, round to oval-shaped adherent cells had become predominant, cells were replated on an ultra low attachment plate, resulting in sphere formation. Spheres were collected and dissociated into single cells by gentle pipetting. Various methods were used to assess the differentiation potential of the sphere-derived cells both in vitro and in vivo.

differentiation of other lineages was not seen (Table 2). During the acquisition of the neuronal phenotype, the cells changed their morphology to that of neuron-like cells (a small cell body with multiple long processes); however, the cells were negative for β-tubulin III and neurofilament M. During the induction of the skeletal myoblasts and cardiomyocytes, no morphological changes were observed and the cells were negative for skeletal myosin and MLC2v. Thus, we generated spheres to select for more primitive cells.

Approximately 3 months after the start of cultivation at a time when small round and oval-shaped cells predominated, adherent cells were capable of forming spheres on ultra low attachment plates. Many cells remained singular or formed small asymmetrical aggregates, but a few days after plating them in ultra low attachment plates, several small spherical clusters of floating cells appeared and thereafter these proliferated to generate larger symmetrical spheres (Fig. 2A). Initially, 13.1±4.2 spheres (range 5–15 spheres, $n=5$) were obtained from 5×10^5 adherent cells. Each sphere was composed of 375±63 cells (range 300–450 cells, $n=10$). Spheres were isolated, dissociated mechanically by gentle pipetting, and cultured again in fresh complete medium in standard tissue culture dishes. The shape of the sphere-derived cells was not homogeneous: cells were predominantly small (15–20 μm in diameter), round or oval-shaped (Fig. 2B), but medium-sized spindle- and star-shaped cells were also seen. No large flat fibroblastic cells were observed after dissociation of the spheres. Sphere-derived cells subsequently proliferated in adherent cultures, and adherent cells from a single sphere could generate multiple new spheres under non-adherent conditions.

Flow cytometry of sphere-derived cells

For comparison with classic MSCs, we examined the surface epitopes of sphere-derived cells and found that they were strongly positive for Sca-1, CD13, CD29, CD44, CD49f, and CD105, weakly positive for CD34 and H-2K^k (MHC class I) (Fig. 2C), and negative for all hematopoietic markers, namely, CD45 and Ter119 (Fig. 2C), and CD4, CD8, Gr-1, CD11b/Mac-1, CD45R/B220, and c-kit (data not shown). In addition, no expression of CD31, VE-cadherin, Flk-1, Thy1.2, and I-A^k (MHC class II) was detected (data not shown). These cell surface profiles indicated that sphere-derived cells were phenotypically similar to classic MSCs [10] except for the expression patterns of CD34, c-kit, Flk-1, and Thy1.2.

Table 2 – Adherent cells without passing through the sphere formation step were not induced into neuron-like cells, skeletal myoblasts, nor beating cardiomyocytes

Lineages	Assessments	Total trials	Positive results
Adipocytes	Oil-Red O staining	5	5
Osteoblasts	ALP staining	5	5
Chondrocytes	Alcian blue staining	10	2
Neurons	β-Tubulin III (Cy3)	30	0
	Neurofilament-M (RT-PCR)		
Skeletal myoblasts	Skeletal myosin (DAB)	30	0
Cardiomyocytes	MLC2v (DAB)	30	0

Each experiment was performed as described in material and methods. Without sphere formation, the adherent cells before sphere formation step could differentiate into adipocytes, osteoblasts, and chondrocytes, as assessed by Oil red O staining, alkaline phosphatase staining, and Alcian blue staining, respectively. In neuronal induction, they acquired the morphology of neuron-like cells but were immunonegative for β-tubulin III and did not express neurofilament-M in RT-PCR analysis. In skeletal myoblastic and cardiomyocytic differentiation, cells did not acquire characteristic morphology and were negative for DAB staining with skeletal myosin and MLC2v.

In vitro phenotypic acquisition of three classical mesenchymal lineages by sphere-derived cells

To characterize sphere-derived cells, we first analyzed their differentiation potential into three classical mesenchymal cell types. One week after adipogenic induction, morphologic changes as well as formation of intracellular lipid vacuoles were noticeable. The vacuoles became larger by day 21 (Fig. 3A) as shown clearly by Oil-red O staining (Fig. 3B), and 23.6±6.8% of the cells were positive ($n=3$). RT-PCR showed expression of two adipocyte marker genes, peroxisome proliferator-activated receptor γ (PPARγ) and adipocyte P2 (aP2), in differentiated cells (Fig. 3C).

Acquisition of the osteoblastic property was followed by alkaline phosphatase staining (Fig. 3D), which showed that 12.6±3.7% of the cells were positive ($n=3$). Von Kossa staining showed the presence of a mineralized matrix (Fig. 3E). RT-PCR analysis confirmed the osteogenic property by showing an increase in the expression of osteoblastic-specific factor-2 (osf2) and induction of osteocalcin (OCN) in the differentiated cells (Fig. 3F).

Induction of the chondrogenic property resulted in acquisition of the characteristic morphology (Fig. 3G) [29] and sulfated proteoglycans as detected by Alcian blue staining (Fig. 3H), and 3.4±2.1% of the cells was positive ($n=3$). RT-PCR showed expression of SOX9 and collagen type II (col II) in differentiated cells (Fig. 3I).

Expressions of PPARγ, osf2, and SOX9 were already be detectable, although weakly, before adipogenic, osteogenic, and chondrogenic induction (Figs. 3C, F, I) respectively, and the expression of these markers increased after these inductions. On the other hand, expression of aP2, OCN, and col II could not be detected before the induction of each phenotype, but the cells tested positive for these markers after each induction. Five experiments were performed for each of these classical mesenchymal differentiations, and the same results were obtained in each experiment.

In vitro acquisition of the neuronal phenotype by sphere-derived cells

We examined the differentiation capability of sphere-derived cells into lineages other than the three classical mesenchymal cell types. For investigation of the differentiation potential into the neuronal lineage, the cells were seeded at a low density and cultured in serum-free medium with EGF and bFGF, followed by stimulation with retinoic acid and NGF. After 12 days of differentiation, adherent cells acquired the morphology of neurons, displaying a cell body

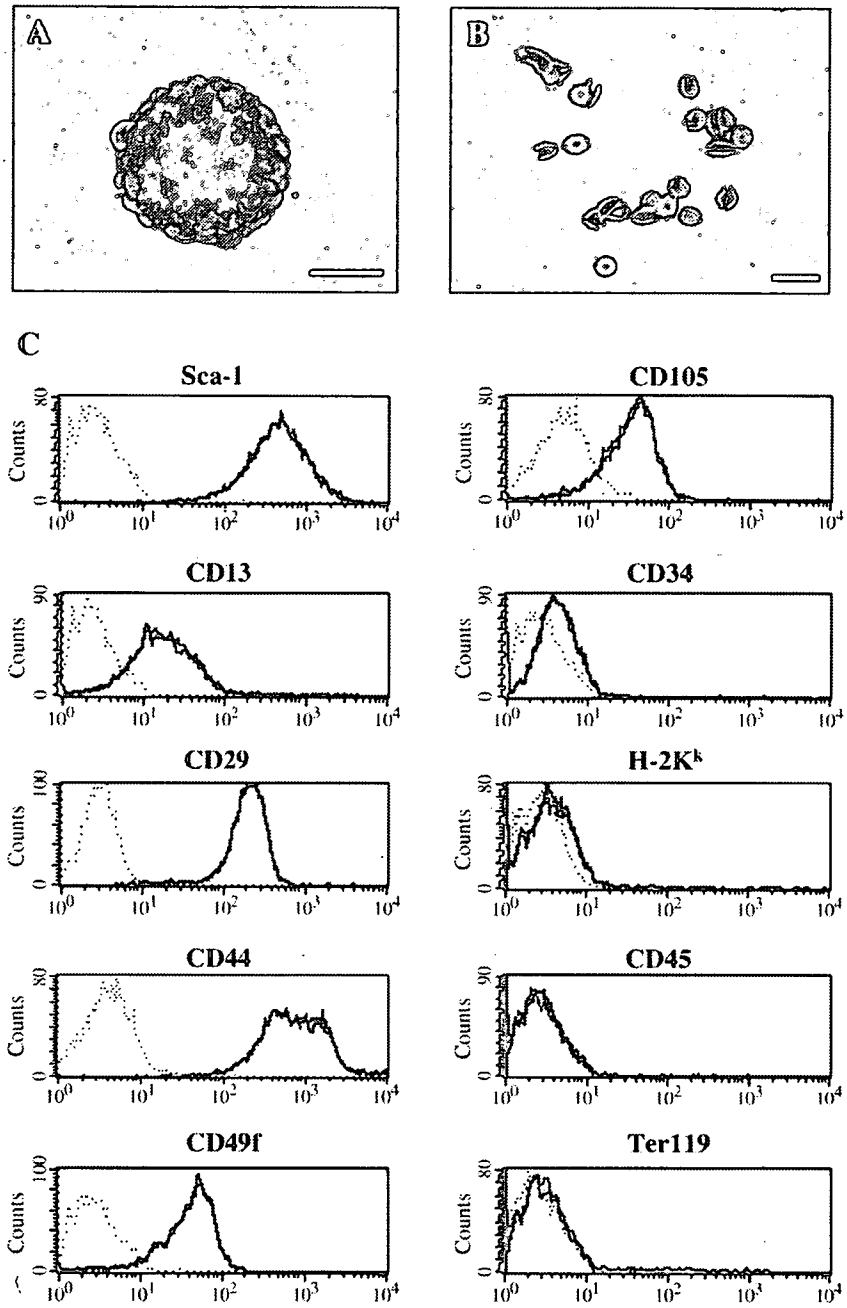

Fig. 2 – Characteristics of isolated cells. Morphology of a sphere 7 days after suspension in ultra low attachment plates (A) and of adherent cells after sphere dissociation (B). All scale bars represent 50 μm. Sphere-derived cells were labeled with antibodies against CD13, CD29, CD34, CD44, CD45, CD49f, CD105, H-2K^k, Sca-1, and Ter119 and analyzed by flow cytometry (C). The dotted thin line indicates the isotype control IgG-staining profile and the thick line the antibody-staining profile. Representative results from one of three independent experiments are shown.

with extended processes and a network-like structure in areas of higher cell density (Fig. 4A). Immunofluorescent assays on cells with phenotypic changes showed staining for nestin (Fig. 4B) and β-tubulin III (Fig. 4C) on day 12 of induction, and 51.2±28.3% of cells were positive for β-tubulin III ($n=3$), but negative for glial-fibrillary acidic protein (data not shown). RT-PCR analysis detected weak expression of nestin before induction and an increase in expression after neuronal induction (Fig. 4D). Expression of neurofilament M was detected only in cells displaying phenotypic changes (Fig. 4D).

Five experiments were performed for neuronal induction, and the same results were obtained in four of these. In one trial, neuron-like cells formed but could not be stained with β-tubulin III in the immunofluorescent assay and failed express neurofilament M as shown by RT-PCR analysis. In the other four experiments, these two assays yielded the same positive results.

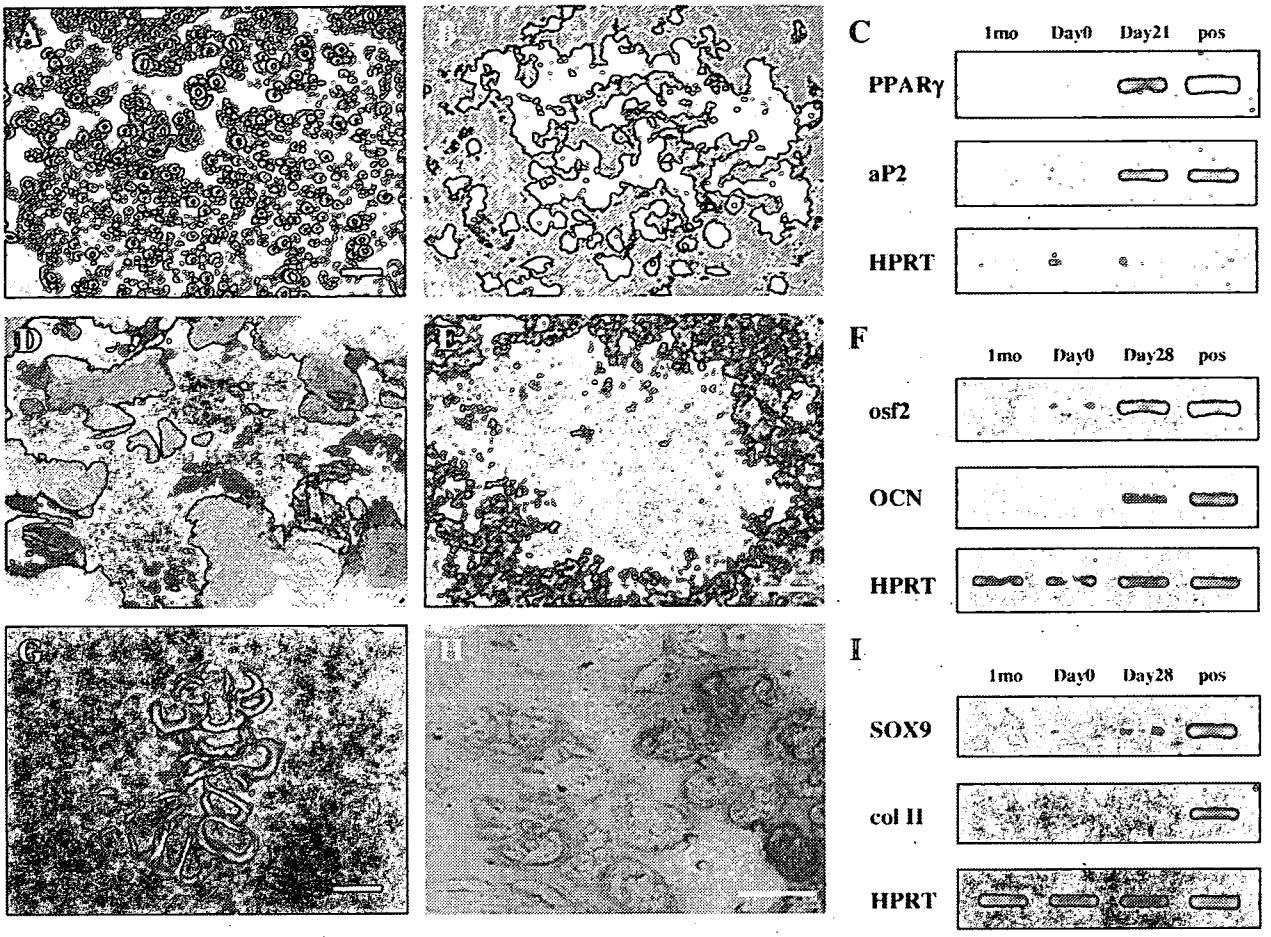

Fig. 3 – Sphere-derived cells acquired phenotypic properties of adipocytes, osteoblasts, and chondrocytes. The adipogenic property was shown by the presence of intracellular lipid vacuoles (A), Oil red O staining (B) and the expression of adipocyte-specific genes (C) after 21 days of induction. The osteogenic property was demonstrated by alkaline phosphatase staining (D), von Kossa staining (E), and the expression of bone-specific genes after 4 weeks of induction (F). The chondrogenic property was demonstrated by the characteristic morphology (G), Alcian blue staining (H), and expression of chondrocyte-specific genes after 28 days of induction (I). All scale bars represent 50 μm. 1 mo: 1 month after starting cultivation; Day 0 and Day 28: before and 28 days after induction of differentiation; pos: positive control (C and F: limb buds of an 18.5-dpc murine embryo; I: limb buds of a 16.5-dpc murine embryo).

In vitro phenotypic acquisition of skeletal myoblasts by sphere-derived cells

Differentiation into skeletal myoblasts was induced *in vitro* by stimulating confluent sphere-derived cells with 5-aza-2′-deoxycytidine. After 14 days, round cells appeared and became elongated (Fig. 4E) to form multinucleated myotubes (Fig. 4F), which then fused together. They were positive for DAB staining of skeletal myosin (Fig. 4F) and desmin (Fig. 4G), and 0.013±0.0021% of cells was positive for myosin ($n=3$). RT-PCR analysis demonstrated that the skeletal myogenic marker genes, myoD and myogenin, were expressed in cells showing phenotypic changes (Fig. 4H). MyoD, but not myogenin, was expressed weakly even before skeletal myogenic induction (Fig. 4H). Five experiments were performed for the phenotypic acquisition of skeletal myoblasts and the same results were obtained in all five experiments.

In vitro phenotypic acquisition of cardiomyocytes by sphere-derived cells

Cardiomyocytic differentiation was also induced in vitro by culturing confluent cells under the same conditions as for skeletal myoblasts. After a longer period, that is, after about 3 weeks, beating ball-like cells appeared (Fig. 4I), and these became connected and elongated to form beating myotubes on day 28 (Fig. 4J). The beating ball-like cells and myotubes were positive for DAB staining of MLC 2v (Fig. 4K) and 0.0043± 0.00086% of the cells were positive for MLC2v ($n=3$), but not for ANP (data not shown). RT-PCR analysis showed that the beating cells were positive for MLC2v and Nkx2.5 and negative for MLC2a (Fig. 4L). None of these markers were expressed before cardiomyogenic induction (Fig. 4L). These patterns demonstrated phenotypic acquisition of ventricular properties because MLC2v is specifically expressed in ventricular cells [30] whereas expression of MLC2a is restricted to the

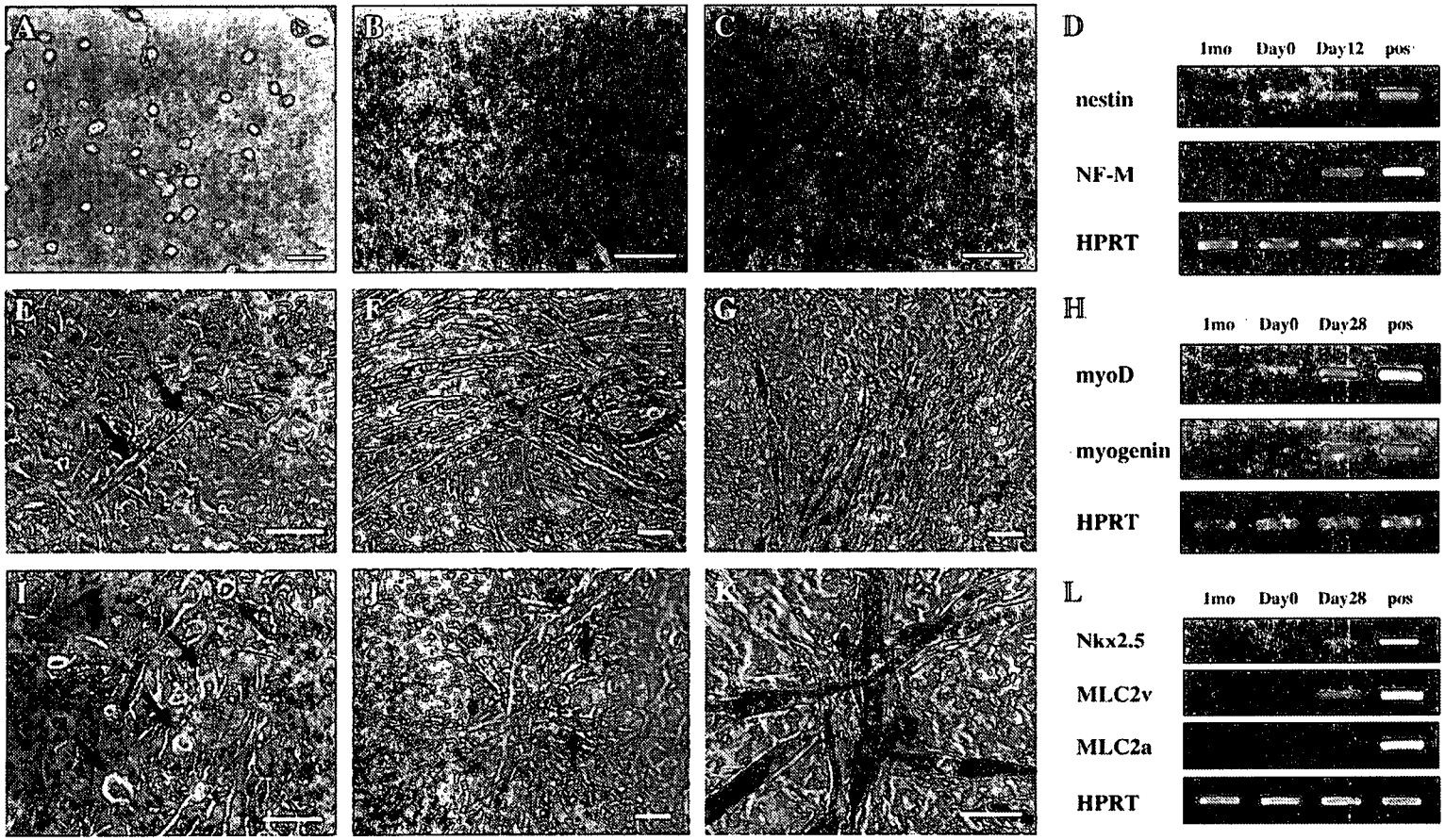

Fig. 4 – Sphere-derived cells acquired phenotypic properties of neurons, skeletal myoblasts, and cardiomyocytes. The neuronal property was demonstrated by the characteristic morphology and network structure after 12 days of induction (A), immuno-positivity for nestin (B) and β-tubulin III (C), and expression of appropriate markers (D). The skeletal myoblastic property was demonstrated by the formation of elongated multinucleated myotubes on day 14 (E, arrows) and day 28 (F, G) of induction, by DAB staining of skeletal myosin (F) and desmin (G), and by expression of skeletal muscle-specific genes (H). The cardiomyocytic property was evidenced by the appearance of beating round cells on day 21 (I, arrows) and beating myotubes on day 28 of induction (J, arrows; K), by DAB staining of MLC2v (K), and by expression of cardiomyocyte-specific genes (L). All scale bars represent 50 μm. 1 mo: 1 month after starting cultivation; Day 0, Day 12, and Day 28: before, 12 days after, and 28 days after induction of differentiation respectively; pos: positive control (D: whole brain of an 18.5-dpc murine embryo; H: limb buds of an 18.5-dpc murine embryo; L: whole heart of a 4-month-old mouse).

atrial myocardium [31]. Five experiments were performed for the acquisition of the cardiomyocytic phenotype, and the same results were obtained in four of these. In one experiment, no beating cardiomyocytes were obtained.

A single marrow-derived sphere expresses nestin and several mesodermal precursor markers and is composed of a heterogeneous cell population

In vitro differentiation assays showed that sphere-derived cells could acquire the phenotypic properties of mesodermal (three classical mesenchymal cell types, skeletal myoblasts, and cardiomyocytes) and ectodermal (neurons) lineages. To determine whether a sphere expresses the markers of precursors of such lineages as well as other more primitive markers, we subjected a single sphere to RT-PCR analysis as shown in Fig. 5A. Spheres neither expressed undifferentiated ES cell markers, Oct-4 [32], or Rex1 [33], nor markers of the primitive mesoderm such as Brachyury [34] (Fig. 5A). However, a single sphere was positive for the neural precursor marker, nestin [40] (Fig. 5A). It also expressed transcription factor markers that are specific to the differentiation of three classical mesenchymal cells (PPARγ [35], osf2 [36], and SOX9 [37]) and skeletal myoblasts (myoD [38]) but did not express Nkx2.5 [39], a marker of cardiomyocyte differentiation (Fig. 5A).

In all cases, expression of these markers was maintained until induction of differentiation (Figs. 3C, F, I and 4D, H, L) and the sphere-derived cells showed multipotency as described above (Figs. 3A–B, D–E, G–H; Figs. 4A–C, E–G, I–K). Five experiments were performed, and each experiment gave similar results.

For a better understanding of the nature of spheres, we performed immunofluorescent analysis of a single sphere for nestin, which has been reported to be expressed in many multipotent spheres obtained from non-neural tissues [16,41,43]. As shown in Figs. 5B–E, most cells composing the sphere were weakly positive for nestin, but some cells located in the peripheral zone of a sphere expressed higher levels. This heterogeneous expression pattern was shared with other spheres ($n=22$). In contrast to spheres, adherent cells that had not undergone sphere formation were mostly nestin-negative, and only extremely weak expression was observed for a small portion of these cells ($1.8\pm0.54\%$, $n=3$, data not shown). These findings indicate that spheres neither correspond to a population of pluripotent ES cells nor to a primitive mesoderm, but rather constitute either a collection of multipotent progenitors of mesodermal and neural lineages at different differentiation stages, a diverse population of monopotent precursors, or a mixture of both.

To distinguish between these possibilities, we attempted single cell cloning of spheres by plating at a density of one cell per 2 wells of a 96-well plate and marking wells with single clones. In thirty 96-well plates, we identified several multipotent clones that were capable of acquiring the phenotypic properties of adipocytes, osteoblasts, chondrocytes, and skeletal myoblasts, in addition to monopotent clones of these lineages (data not shown). However, fully multipotent clone or monopotent clones of neurons or cardiomyocytes were not isolated. In theory, the multipotentiality of the spheres characterized here could be explained by the presence of a mixture of monopotent precursors of 6 cell types. However, if this were the case, all 6 cell types should have been obtained by single cell cloning, which was not the case.

To understand the role of the sphere-formation step, we performed RT-PCR analysis of all the markers examined in Fig. 5A and characterized the differences between spheres (Fig. 6, lane A), non-spheres, (Fig. 6, lane B), and the two clones obtained after single cell cloning (Fig. 6, lane C and D). Non-spheres did not express myoD, and compared to spheres, expressions of PPARγ, osf2, SOX9, and nestin were weaker (Fig. 6, lane B). These results indicated that spheres and non-spheres were composed of different cell populations. Judging from the results of the phenotypic differentiations shown in Table 2 and Figs. 3 and 4, spheres contained multipotent cell populations that were capable of generating more phenotypes than the cell population of non-spheres did. Clone 1 acquired the phenotypes of adipocytes, osteoblasts, and skeletal myoblasts and weakly expressed nestin in addition to precursor markers of each of these lineage (PPARγ, osf2, and myoD) (Fig. 6, lane C). Monopotent clone 2, which could differentiate into adipocytes, only expressed PPARγ (Fig. 6, lane C). These results indicated that the sphere-forming step favored for the acquisition of nestin-positivity and multipotency, which was impossible for the non-spheres in our method. In contrast, in single cell cloning, the expression of nestin regressed as clones lost their multipotency.

Therefore, we conclude that multipotent progenitors with the capacity to acquire phenotypic properties of neurons and/or cardiomyocytes as well as those of several mesenchymal cell lineages were generated by our method.

In vitro engraftment of sphere-derived cells as cardiomyocytes and functional improvement in the myocardial infarction model

In order to determine if sphere-derived cells could repair damaged tissues, we first tagged them with eGFP, which showed that the efficacy of retroviral transduction ranged between 38% and 72% (Fig. 7A). After the GFP^+ cells had been sorted by FACS Vantage, sphere-derived cells were pretreated with 5-aza-2′-deoxycytidine and injected into the myocardium of an AMI model mouse.

Cardiac catheterization was performed 1 month later to determine whether transplantation of sphere-derived cells had a functional impact. LV systolic performance as assessed by LV +dP/dt in AMI (Fig. 7Bb) and PBS (Fig. 7Bc) groups decreased to 57.5% and 60.5% of that of normal control (Fig. 7Ba), respectively. Transplantation of 1×10^6 sphere-derived cells (Fig. 7Bd) resulted in a reduction of LV +dP/dt to 32.4% of that of normal control, which was a significant improvement compared with both PBS and AMI groups. The assessment of LV −dP/dt also showed a significant improvement in the cell-transplanted group compared with PBS and AMI groups (data not shown). Assessment of LV diastolic performance showed deterioration of LVEDP in all groups, but compared with PBS and AMI groups the LVEDP of cell-transplanted group was much better (Fig. 7C).

Immunofluorescent staining 28 days after surgery showed that GFP^+ cardiomyocytes were detected in all five experi-

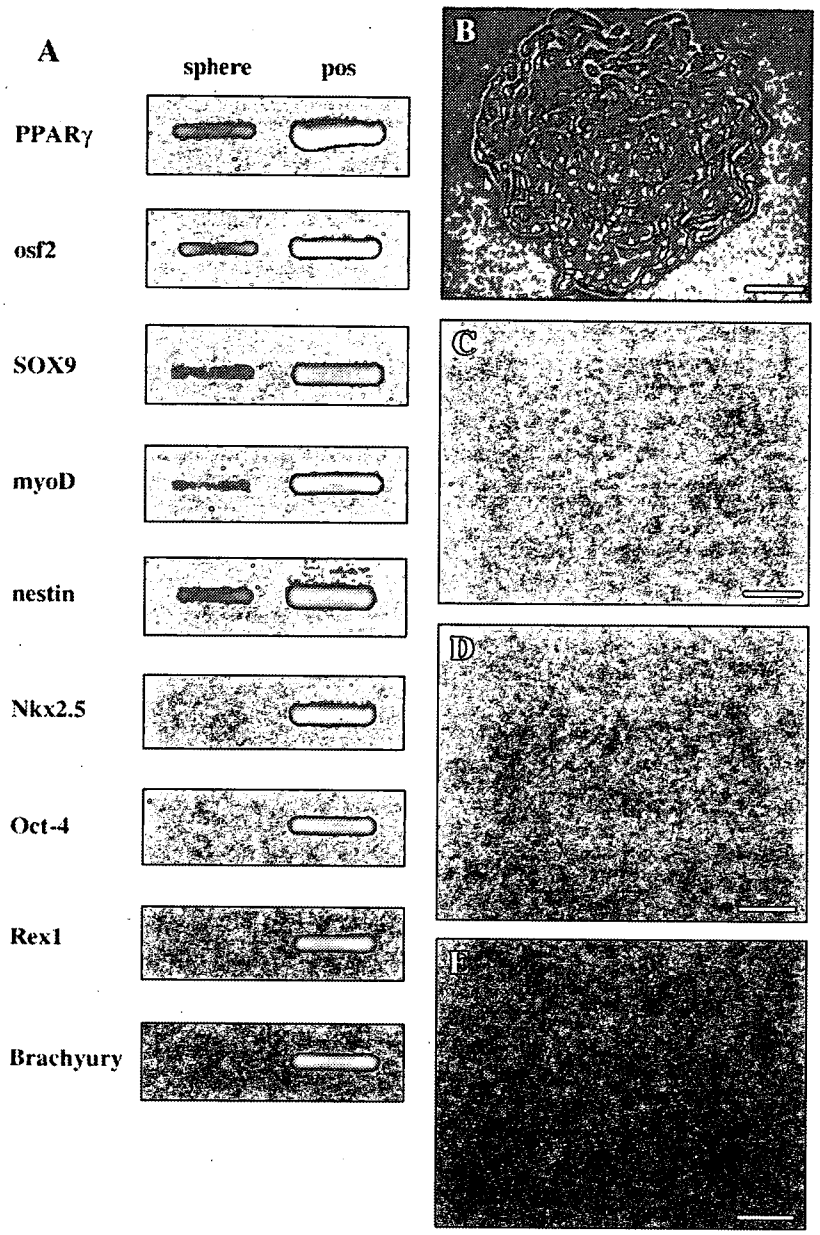

Fig. 5 – Characteristics of a single sphere. (A) RT-PCR analysis of a sphere shows the transcription factors expressed during differentiation into three classical mesenchymal lineages (PPARγ, osf2, SOX9) and skeletal myoblasts (myoD), and the presence of a neural progenitor marker, nestin. The transcription factors of cardiomyocytes (Nkx2.5), undifferentiated ES cells (Oct-4, Rex1), and primitive mesoderm (Brachyury) were not expressed in the sphere. Sphere: a floating sphere 7 days after suspension in an ultra low attachment plate; pos: positive control (Oct-4 and Rex1: undifferentiated murine ES cells; Brachyury: murine embryo at 7.5 dpc; others: described in Figs. 3 and 4). (B–E) Immunofluorescent analysis of nestin in a sphere. The heterogenous expression patterns were similar with each other (n=22). All scale bars represent 50 μm. (B: bright field; C: Hoechst33352; D: nestin-Cy3; E: merged image).

ments (see Figs. 7D–G for a representative experiment). GFP^+ cells were detectable in peri-infarction zones (Figs. 7D, E) and simultaneously expressed cardiac troponin I (Figs. 7F, G) and tropomyosin (data not shown). We searched for GFP positive cells from the apex to the base of the transplanted heart and found 6.8±2.6 (n=5) cells per heart. Considering the number of injected cells (1×10^6 cells per mouse), the frequency of the cells engrafted as cardiomyocytes was very low (less than 0.001%).

Next, we evaluated angiogenesis by immunofluorescent analysis with CD31 (Fig. 7H). Increases in capillary numbers were observed at the peri-infarct zone in mice injected with sphere-derived cells. All CD31-positive cells were GFP-negative. Compared with PBS-injected (22.4±4.51 vessels) and AMI (25.4±7.30 vessels) groups, the cell-transplanted group (37.2±8.79 vessels) showed a marked increase ($0.01<p<0.05$) in CD31-positive vessels. No tumor formation was found in these experiments.

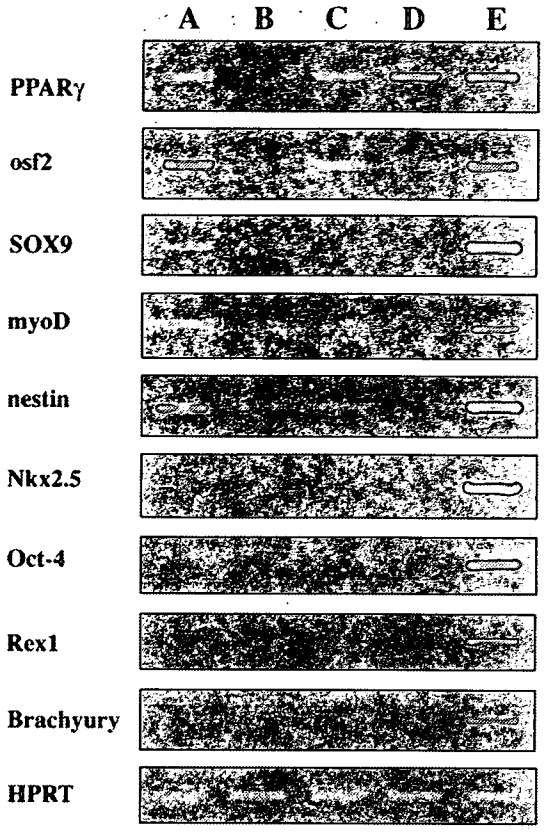

Fig. 6 – RT-PCR analysis of spheres, non-spheres, and two clones. Spheres (A) showed different expression patterns of PPARγ, osf2, SOX9, myoD, and nestin, compared to non-spheres (B). Multipotent clone 1 (C) expressed the precursor markers of each lineage (PPARγ, osf2, myoD) and nestin weakly. Monopotent clone 2 (D) expressed only PPARγ. (A: floating spheres 7 days after suspension on an ultra low attachment plate; B: non-spheres; C: clone 1; D: clone 2; E: positive control as described in Fig. 5).

These results showed that sphere-derived cells could be engrafted as cardiomyocytes only at low frequency *in vivo*, but stimulated host angiogenesis, and significantly improved cardiac function in the AMI model.

Discussion

This study describes a method, based on sphere formation, which allows the isolation of a murine marrow-derived multipotent cell population that is capable of acquiring the phenotypic properties of adipocytes, osteoblasts, chondrocytes, neurons, skeletal myoblasts, and cardiomyocytes. The multipotent cell population also showed cardiomyogenic potential *in vivo* and had beneficial functional effects in an AMI model. To the best of our knowledge, this is the first evidence that multipotent spheres can be generated from bone marrow.

Without sphere formation, the culture conditions of adherent cells principally resembled those of MSCs that have been repeatedly shown to be pluripotential [3,10,25,42]. However, unlike MSCs, non-spheres in our method could not acquire phenotypes other than those of classical mesenchymal lineages. As the isolation of MSCs from murine bone marrow has been reported to be difficult [15], the conflicting results might be due to the differences in the isolation methods; strains of mice used (C3H/He) [15], starting cell populations (lineage negative marrow cells obtained with Dynabeads), and/or source of FCS (no check to support the growth of MSCs).

After forming spheres, cells acquired the phenotypic properties of multi-lineages. Immunofluorescent analysis showed that in contrast to most non-spheres, spheres expressed nestin, which was also confirmed by RT-PCR analysis, and were composed of a mixture of heterogeneous cell populations. Nestin has been reported in spheres of multipotent stem/progenitor cells of many non-neural tissues [16,41,43] and is suggested to be a marker of stem cells or an indicator of plasticity [41]. Moreover, only nestin-positive marrow stromal cells in rats were capable of forming spheres under specific culture conditions and differentiating into ectodermal lineage [47]. Therefore, spheres in our method might have acquired multipotency through enhanced expression of nestin.

Lots of recent reports on murine MSCs also showed immunopositivity for nestin [41,44,45], but its expression in MSCs seems to be still subject to some controversy [44] The reported percentage of nestin-positive murine MSCs ranges widely from 3.1% to nearly 100%, whereas others have reported little expression [46]. Serum has been reported to inhibit nestin expression in rat marrow stromal cells [47], although most MSCs have been cultured in serum-rich medium and found to express nestin. These discrepancies could be also partially due to differences in isolation methods.

We suggested that our spheres could consist of four cell populations: multipotent stem/progenitor cells similar to those obtained from other tissue-derived multipotent spheres, multipotent precursors at different stages of differentiation, monopotent precursors of several lineages, or a mixture of these. To distinguish between these possibilities, we tried single cell cloning of a marrow-derived sphere, but could not isolate a multipotent clone capable of phenotypic acquisition of all 6 cell types or capable of producing monopotent clones of neurons or cardiomyocytes (data not shown). Several factors may account for our failure to establish fully multipotent clones. First, paracrine factors secreted by surrounding cells might be important for maintaining multipotentiality. Second, the acquired phenotypes of neurons and cardiomyocytes might be more easily lost when marrow stromal cells are used rather than other cell types. Third, we cannot exclude the possibility of technical problems. The frequency of fully multipotent progenitors might be small, which could have resulted in their loss during cloning. Alternatively, cell damage, greater than that after gentle pipetting, may have occurred when the pellets were dissociated vigorously into single cells at the time of cloning. In fact, we could not obtain a fully multipotent cell population when the spheres were dissociated by vigorous pipetting.

Despite these issues, our sphere-derived cells differ from classical murine MSCs and other marrow-derived stem/progenitor cells [2,13–15,48] as they displayed the phenotypic